Characterization of total ecosystem scale biogenic VOC exchange at a Mediterranean oak-hornbeam forest

S. Schallhart[1], P. Rantala[1], E. Nemitz[2], D. Taipale[1,3,4], R. Tillmann[5], T. F. Mentel[5], B. Loubet[6], G. Gerosa[7], A. Finco[7], J. Rinne[1, 8,9,10], and T. M. Ruuskanen[1]

[1]{Department of Physics, University of Helsinki, Helsinki, Finland}

[2]{Centre for Ecology & Hydrology (CEH), Penicuik, United Kingdom}

[3]{Department of Plant Physiology, Estonian University of Life Sciences, Tartu, Estonia}

[4]{University of Helsinki, Department of Forest Sciences, University of Helsinki, Helsinki, Finland}

[5]{Forschungszentrum Juelich GmbH, Juelich, Germany}

[6]{National Institute of Agronomic Research UMR ECOSYS INRA, AgroParisTech, Université Paris Saclay, France}

[7]{Department of Mathematics and Physics, Catholic University of Brescia, Brescia, Italy}

[8]{Department of Geosciences and Geography, University of Helsinki, Helsinki, Finland}

[9]{Finnish Meteorological Institute, Helsinki, Finland}

[10]{Department of Physical Geography and Ecosystem Science, Lund University, Lund, Sweden}

Correspondence to: S. Schallhart (simon.schallhart@helsinki.fi)

Abstract

Recently, the number and amount of biogenically emitted volatile organic compounds (VOCs) has been discussed vigorously. Depending on the ecosystem the published number varies between a dozen and several hundred compounds. We present ecosystem exchange fluxes from a mixed oak-hornbeam forest in the Po Valley, Italy. The fluxes were measured by a proton transfer reaction-time-of-flight (PTR-ToF) mass spectrometer and calculated by the eddy covariance (EC) method. Detectable fluxes were observed for up to 29 compounds, dominated by isoprene, which comprised over 60% of the total upward flux (in molar basis). The daily average of the total VOC upward flux was 10.4 nmol m^{-2} s^{-1}. Methanol had the highest concentration and accounted for the largest downward flux. Methanol seemed to be deposited to dew, as the downward flux happened in the early

morning, right after the calculated surface temperature came closest to the calculated dew point temperature.

We estimated that up to 30% of the upward flux of methyl vinyl ketone (MVK) and methacrolein (MACR) originated from atmospheric oxidation of isoprene. A comparison between two methods for the flux detection (classical and automated) was made. Their respective advantages and disadvantages were discussed and the differences in their results shown. Both provide comparable results.

1. Introduction

Volatile organic compound- fluxes between vegetation and atmosphere affect atmospheric chemistry by controlling the oxidation capacity of the atmosphere (Fehsenfeld et al., 1992, Fuentes et al., 2000). The non-methane biogenic VOC emissions are dominated by terpenoids, e.g. isoprene and monoterpenes, followed by oxygenated VOCs such as methanol and acetone (Kesselmeier et al., 1999, Guenther et al., 2012). The emitted VOCs are physically removed by dry or wet deposition or are oxidized by e.g. OH, O_3 and NO_3 (Mogensen et al., 2015). Their oxidation contributes to the tropospheric ozone formation and destruction processes (e.g. Derwent et al., 2003, Bloss et al., 2005), aerosol formation and aerosol growth and, thereby, influences air quality and climate (Kulmala et al. 1998, Tunved et al., 2006, Monks et al., 2009, Riipinen et al., 2012, Paasonen et al., 2013). To assess these effects caused by the biogenic VOCs, reliable flux budgets are necessary.

Most ecosystem scale VOC flux measurements have been conducted with disjunct eddy covariance method by mass scanning using proton-transfer-reaction quadrupole-mass-spectrometer (PTR-QMS), relaxed eddy accumulation or surface layer gradient techniques with gas chromatography - mass spectrometry applying selected ion mode (e.g. Lamb et al., 1985; Businger and Oncley, 1990; Fuentes et al., 1996; Guenther et al., 1996; Rinne et al., 2001; Karl et al., 2002; Rinne and Ammann, 2012). These methods require pre-selection of target compounds and in case of the PTR-QMS suffer from the limitation of unit mass resolution, making it impossible to separate isobaric compounds, i.e. compounds with identical integer mass, but different chemical composition. Thus, measurements have inherently focused on compounds already known to be emitted by vegetation and thereby hinder the discovery of fluxes of compounds not previously known to be emitted by vegetation. Furthermore, extreme weather conditions such as hail can change the VOC flux pattern (Kaser et al., 2013), which is difficult to measure with such methods.

Lately, new insights were provided by the more universal and sensitive PTR-ToF. Park et al. (2013) analysed flux data obtained by the PTR-ToF and revealed many previously unobserved compounds to be emitted, but this approach has so far only been applied to very few vegetation types (e.g. Ruuskanen et al., 2011, Park et al., 2013, Kaser et al., 2013).

In this study we have conducted VOC flux measurements at a remnant natural oak-hornbeam dominated forest (Bosco Fontana) in northern Italy as part of an intensive field campaign organized by the European FP7 project 'ÉCLAIRE' (Effects of climate change on air pollution impacts and response strategies for European ecosystems). The objectives of the ÉCLAIRE Bosco Fontana experiment were (a) to quantify the exchange of a range of pollutants with this ecosystem in one of the most polluted regions of Europe, (b) to assess the importance of in-canopy chemical interactions on the biosphere / atmosphere exchange of reactive gases and aerosols and (c) to provide a supersite in the framework of a spatial Po Valley study that combined resources from two EU projects (ÉCLAIRE, PEGASOS: Pan-European gas aerosol climate interaction study) with a national Italian initiative.

In this paper, we present the results of the application of state-of-the-art PTR-ToF mass spectrometry and eddy covariance technique to derive the total biogenic VOC flux above the Bosco Fontana ecosystem. The aims of this study were: i) the comparison of two data processing approaches to identify compounds for which fluxes were above the detection limit, contrasting the automated method used by Park et al. (2013) with the "classical" method, which is using manual cross covariance peak checking (e.g. Taipale et al., 2010; Ruuskanen et al., 2011; Kaser et al., 2013); ii) the characterization of the total ecosystem scale VOC flux from a Mediterranean oak forest, with particular emphasis on iii) the quantification of the contribution of non-terpenoid VOCs to the total VOC flux, iv) the estimation of the possible contribution of secondary compounds to the observed above-canopy fluxes, and v) the study of dew potentially causing methanol deposition in the morning. A companion paper (Acton et al., 2015) compares the PTR-ToF-MS measurements with simultaneous measurements by PTR-QMS and a bottom-up estimate of the canopy flux scaled up from leaf level emission measurements, and also derives emission factors for the use in emissions models.

2. Materials and methods

2.1. Bosco Fontana site description

The measurements were performed from June 15th to July 6th 2012 in Bosco Fontana, Lombardy, Italy. Bosco Fontana is a 233 ha forested nature reserve located in the north-east of the Po valley. The main tree species are *Quercus cerris* (turkey oak), *Quercus robur* (pedunculate oak), *Quercus rubra* (northern red oak) and *Carpinus betulus* (Hornbeam) (Dalponte et al., 2008). The typical height of the trees varied between 26 and 28 m. The surroundings of the Bosco Fontana forest area are

agricultural land and some roads. The largest city nearby is Mantua, with 48000 inhabitants, which is located 8 km to the south-east. The measurement site is 25 m above sea the level. The temperatures varied from 18 to 32 °C during the campaign and the main wind directions were east and west. The measurement tower was 42 m high and located in the south-western part of the nature reserve (45.20°N, 10.74°E). Figure 1 shows a satellite image of the area, with the position of the tower and the mean 80% footprint (Acton et al., 2015). The climatological mean annual temperature is 13.3°C and the mean annual precipitation is 834 mm (Willmott and Matsuura, 2012a and 2012b).

2.2. Meteorological and trace gas data

The measurement tower was equipped with temperature and relative humidity sensors at several heights. The turbulence data were measured with a 3-d anemometer (HS 50, Gill Instruments) at 32 m above ground level (later referred as agl) and the instrument was fastened on a pole 1.7 m away from the lattice tower. An additional measurement of wind direction was provided by a 2-d ultrasonic anemometer as part of an integrated weather station (Weather Transmitter WXT610, Vaisala; 32 m agl), which also measured air pressure, relative humidity and temperature. The O_3 concentration was determined with a chemiluminescence analyser (Model 202, 2B Technologies) at 40 m agl and NO_2 and NO with a chemiluminescence analyser equipped with a thermal converter (Model 42C, Thermo Scientific) at a height of 32 m agl.

Carbon dioxide flux measurements were performed, using the eddy covariance technique, at the top of the tower where a sonic anemometer (USA 1, Metek) and a fast IRGA analyzer (mod. 7500, LICOR) were mounted on a pole, 1.7 m far from the edge of the tower. The sonic anemometer was working at 20 Hz and the fast IRGA was calibrated before and after the field campaign and no significant drift was observed. Carbon dioxide fluxes were measured from June 18th to July 12th. Several procedures were applied in order to obtain the correct flux calculations: despiking (Vickers and Mahrt, 1997), double rotation of the reference system (Kaimal and Finnigan, 1994), linear detrending (Lee at al., 2004), frequency loss corrections using the ogive methodology (Ammann et al., 2006), WPL corrections for density fluctuations (Webb et al. 1980), stationarity test (Foken and Wichura, 1996); finally a manual selection of the data was performed too and data after rainfalls were discarded.

The dew point temperature, T_d, was calculated according to Lawrence (2005):

$$T_\mathrm{d} = T\left[1 - \frac{T\ln\left(\frac{\mathrm{RH}}{100}\right)}{\frac{L_\mathrm{vap}}{R_\mathrm{w}}}\right]^{-1} \quad (1)$$

where T is the ambient temperature, RH is the relative humidity, L_{vap} is the enthalpy of vaporization (2.501 x 10^6 J kg^{-1}) and R_{w} is the gas constant of water vapour (461.5 J K^{-1} kg^{-1}).

The average aerodynamic temperature $T(z_0')$ was estimated using a method described by Nemitz et al. (2009) as

$$T(z_0') = T + \overline{\theta' w'}(R_a + R_b), \quad (2)$$

where z_0' is the notional mean height of the canopy exchange, $\overline{\theta' w'}$ and T are the measured heat flux and temperature at the measurement height of z_{m}, respectively. In this study, the roughness length z_0 was estimated to be ca. 1 m (e.g. Dolman, 1986). For the zero displacement height d we used the common approximation of $d = 2/3 \times z_{\mathrm{c}}$, where z_{c} is the canopy height (28 m).

The resistance parameters R_a and R_b were determined as (Owen and Thompson, 1963; Garland, 1977)

$$R_a = \frac{u}{u_*^2} - \frac{\Psi_h\left(\frac{z_m - d}{L}\right) - \Psi_m\left(\frac{z_m - d}{L}\right)}{k u_*} \quad (3)$$

and

$$R_b = (B u_*)^{-1}, \quad (4)$$

where L is the Obukhov length. The sublayer-Stanton number (B) can be estimated by

$$B^{-1} = 1.45 Re_*^{0.24} Sc^{0.8}, \quad (5)$$

where roughness Reynolds number Re_* is given by

$$\mathrm{Re}_* = \frac{z_0 u_*}{\upsilon} \quad (6)$$

and the Schmidt number Sc by

$$\mathrm{Sc} = \frac{\upsilon}{D} \quad (7)$$

The friction velocity u_* and the horizontal wind u were taken from the measurements at z_m and k is von Karman's constant (0.4). The kinematic viscosity of air, υ, was assumed to be constant ($\approx 1.56 \times 10^{-5}$ m^2 s^{-1}), so was the thermal diffusivity temperature in air, D ($\approx 1.9 \times 10^{-5}$ m^2 s^{-1}). The integral stability correction functions Ψ_h and Ψ_m for heat (h) and momentum (m), respectively, were taken from Rannik (1998).

2.3. VOC measurements

2.3.1 PTR-ToF measurements

The PTR-ToF (Ionicon Analytik GmbH; Graus et al., 2010, Jordan et al., 2009) combines the soft ionization of a PTR source with the high mass resolution of a time of flight of mass spectrometer

~4500 m/Δm (determined as the full width at half maximum of the ion peak). The precise mass of a compound can be derived from the time of flight and the elemental composition can be calculated from the observed mass defect. Therefore the instrument can separate isobaric compounds. It cannot, however, distinguish between isomeric compounds, as it gives no information about the compound structure. The real-time measure of full spectra at 10 Hz allows for flux measurements with the eddy covariance technique.

The PTR-ToF was placed inside a container next to the measurement tower. Air from 32 m height was sampled through a 40 m long and 9.5 mm wide (inner diameter; i.d.) PTFE tube (hereafter referred to as common sampling line), which was pumped at 63 l min^{-1}. The pressure drop induced by the pumping was sufficient to prevent condensation in the sampling line outside of the container. Inside the air conditioned container, the inlet line was heated (self-regulated heating wire with 11 W/m at 30 °C). The 3-d wind measurements were obtained with a frequency of 10 Hz 10 cm above the inlet.

The PTR-ToF was connected to the inlet line via a 3-way valve (type: 6606 with ETFE, Bürkert GmbH & Co. KG), from where a subsample of 0.5 l min^{-1} were pumped through a 1.6 mm (i.d.) and 1 mm (i.d.) PEEK capillary (together around 20 cm long; heated between 40°C and 60°C) to the instrument. The PTR-ToF used a 30 ml min^{-1} flow for analysis, the remaining flow was discarded and served only as a by-pass flow in order to decrease the response time of the PTR-ToF and associated wall losses in the inlet capillaries. The drift tube was operated at 600 V and temperature of 60 °C. Together with a drift tube pressure of 2.3 mbar this resulted in an E_{PTR}/N ratio of 130 Td, where E_{PTR} is the electrical field strength and N is the gas number density. The instrument produced a time series of 22 days, with a 1.5 day break when the air-conditioning in the container failed.

2.3.2 Calibration & concentration calculation

The instrument background was measured one to three times per day. A small pump (N86KNE , KNF Neuberger) established a 1.4 l min^{-1} flow from the common sampling line to a custom made catalytic converter. This converter was heated to 350 °C and created VOC-free (zero-) air at ambient humidity. The zero air was connected to the second port of the three way valve and passed an overflow in order to achieve a constant zero air flow at a constant pressure (Fig. 2). The background measurements were used for the calculations of the concentrations as well as the determination of the limit of detection.

The instrument was calibrated every second week, i.e. a total of three times. A custom build calibration unit, which mixed zero air with the calibration gas, was inserted between the catalytic

converter and the overflow (Fig. 2). The calibration gas (Apel Riemer Environmental Inc.) contained 16 different compounds with the mass range from 33 to 180 amu at known concentrations of around 1 ppm. As the gas was diluted with zero air (calibration gas: 10 ml min^{-1}; zero air: 1.4 l min^{-1}) the resulting mixing ratios were around 7 ppb. The sensitivities were calculated from the observed count rates of the zero air and the calibration gas measurements in the ppb range. For the VOCs that were not included in our calibration standard, we used average sensitivities for compound families C_xH_y (based on isoprene, benzene, toluene, o-xylene, trimethylbenzene, naphthalene, α-pinene combined with $C_6H_9^+$ fragment), $C_xH_yO_z$ (considering acetaldehyde, acrolein, acetone, 2-butanone) and $C_xH_yN_z$ (set to that of acetonitrile). The averaged sensitivities were: C_xH_y = 13 (± 1.7) ncps ppb^{-1}, $C_xH_yO_z$ = 19.1 (± 1.3) ncps ppb^{-1} and $C_xH_yN_z$ = 18.1 (± 1.3) ncps ppb^{-1}. The ranges given in the brackets are the standard deviations of the average sensitivities calculated for the compounds in each group from the calibrations. Normalized counts per second (ncps) have been corrected for transmission (pusher duty cycle losses) and primary ion fluctuations (Herbig et al., 2009). The average signal of the primary ion signal (upscaled via the isotope $H_3{}^{18}O_1^+$) was around 750000 cps (Transmission corrected: 10^7 cps). The impurities were: O_2^+ 4% and NO^+ 0.3% of the H_3O^+ primary ion. The monoterpene sensitivities were derived from the α-pinene calibrations (in the calibration gas). Fragments from compounds in the calibration standard were not taken into account when calculating the sensitivities. For example, the signal at $C_5H_9^+$ (*m/z* 69.0699) relates to the protonated parent ion of isoprene and is scaled up to the total isoprene, although some isoprene fragments also show up at other masses. As a consequence it is important that fluxes at those fragments are excluded to avoid double-counting. The result of this procedure can be found in Table A1.

For compounds/fragments not included in the calibration standard, the average sensitivities for the compound families are applied as previously described. In this case the fragmentation pattern is not accounted for and all fragments have to be added up to arrive at the total flux, excluding those that could be associated with calibrated compounds. Two exceptions were made, as acetic acid was not calibrated, but its major fragment ($C_2H_3O^+$; Baasandorj et al., 2015) was disregarded, the sensitivity for acetic acid was halved (9.55 ncps ppb^{-1}). For ethanol ($C_2H_7O_1^+$) the methanol sensitivity was used. For the data post processing the ToF Analyzer V2.45 software was used, which has been described in Müller et al. (2010 and 2013). A peak list (Table A1) was created with the TofTools software (Junninen et al., 2010), by integrating the 10 Hz raw data for one hour and then fitting and identifying the different peaks. The measured mass peaks were identified by matching them with the calculated masses of different combinations of H, C, O, N and S atoms. The range of atoms allowed to appear in a compound was set from 0 to 50.

After peak fitting was performed on the 10 Hz data the output of the ToF analyzer were aggregated to provide 30 min concentration data in a three-step process: first, the 10 Hz data were averaged over 30 minutes. From these 30 min data the zero air measurements were subtracted, wherein values for the times between the zero air measurements were linearly interpolated. The resulting signals were then compared to the limit of detection LOD = $2\sigma_{\mathrm{zero}}$, where σ_{zero} is the standard deviation of the 10 Hz zero-air signal during a 30 min measurement. To calculate the volume mixing ratios, all compounds above the LOD were divided by the measured or assigned sensitivity. Compounds with signals below the LOD were disregarded from the further analysis (Table A1).

2.3.3 Flux calculations

Fluxes were derived using the eddy covariance (EC) method. In EC, the flux is calculated using a discretized covariance:

$$\overline{w'c'} = \frac{1}{n}\sum_{i=1}^{n} w'(i)c'(i + \lambda/\Delta t), \quad (8)$$

where w' and c' are high frequency fluctuations of vertical wind and concentration, respectively, i the number of the measurement, n is the sum of all measurements during the flux averaging time (30 min in this study), Δt is the sampling interval (0.1 s) and λ is the lag time caused by the sampling tubes (e.g. Kaimal and Finnigan, 1994).

In this study, vertical wind and VOC concentrations were both recorded at 10 Hz frequency. The flux calculation procedure was the following:

First, the wind vector was 2-d rotated using the method described by Kaimal and Finnigan, (1994). If the vertical rotation was more than 5°, the period was flagged and after the 'compound with exchange' detection rejected from further analysis. Data which were measured during periods when the wind was coming through the tower was not filtered out (discussed in Acton et al., 2015).

The linear trend was removed from the concentrations while block averaging was used for the vertical wind measurements.

Next, cross covariance functions (CCFs) were calculated between the vertical wind and each of the volume mixing ratios for every 30 minute measurement period. The lag time and compounds for which the flux was deemed detectable were identified with two different methods (Table 1), which are termed the "classical method" (Taipale et al., 2010) and the "automated method" (Park et al., 2013).

For the classical method the lag time was determined for each 30 min periods and compounds individually by maximizing the smoothed cross covariance function from a lag time window of 0–5

s (Taipale et al., 2010). The smoothing of the CCF decreases possible flux overestimation caused by noise when using the maximum covariance method (Taipale et al., 2010; Langford et al. 2015). In the next step compounds with detectable flux were identified by checking the cross covariance functions manually for each individual compound and for several different 30 min periods. The total number of manually identified CCFs was well over 1000. Compounds for which a clear CCF maximum was found were used for the further flux calculations.

For the automated method, such as in Park et al. (2013), a constant lag time (2.6 s) was used for all compounds and all 30 min measurement points. This avoids overestimation in the flux, which can happen if the maximizing method is used for flux values close to the detection limit (Langfold et al., 2015). This lag time used here was calculated from the averaged absolute cross covariance function of isoprene, which exhibits a clear maximum. The individual 30 min lag times from the selected time window were also calculated to confirm that the lag time did not shift during the campaign. To identify the compounds with detectable flux, an automated flux searching routine was used. First, absolute CCFs for each compound were calculated using daytime values from 10:00 to 16:00 (CET), i.e. when good conditions for turbulence and high flux are present (see Fig A5; Park et al., 2013). Next, the absolute values of the 30 min CCFs in this time window were averaged over the entire measurement period (Fig. A6 to A9). From this averaged CCF, the routine automatically calculated the flux (at 2.6 s lag time), the average noise and the standard deviation of the noise (σ_{noise}). The mean and standard deviation of the noise were determined from areas at the left and right border of the CCF spectra (Fig A6 to A9). Finally, the mean noise was subtracted from the flux and then divided by σ_{noise}. For ratios >3 the respective compound was used for the further flux calculations.

The final flux values were calculated for each method from the original (not smoothed or absolute) 30 min CCFs by using the respective lag time and compound. The fluxes of both methods were then filtered using the stationarity criteria introduced by Foken and Wichura, (1996): every 30 min period was divided into six 5 minute sub-periods and VOC fluxes were calculated for each 5 min period. If the flux values calculated using 5 min averages differed by more than 30%, the period was disregarded from further analysis. The stationarity criteria together with the 5° tilt angle disregarded 43% of the data for each method.

For those compounds for which a flux could be detected, the uncertainty of the flux was calculated from the two 60 s time windows at the border of the CCFs for each 30-minute flux value. The root mean square of each window was calculated and the results averaged. This follows the approach of Langford et al. (2015) and ensures that offsets (from zero) from the noise in the CCF tails are taken into account. For estimation of the uncertainty of the diurnal net flux, it was assumed that the errors of different flux values are independent, and the uncertainty can be calculated with the Gaussian

propagation of error. The independence assumption is not fully correct, as fluxes from different compounds are derived using the same vertical wind data.

For the calculation of the diurnal 1 h flux data, all measurements which passed the quality checks were averaged. The daily average was then calculated by averaging the diurnal data. This ensures that periods, which have fewer data points (due to quality criteria filtering, background or calibration measurements) do not get underrepresented in the daily average.

2.3.4 Spectral corrections

Due to the high frequency attenuation and low frequency cutoff, the measured EC flux underestimates the real flux (e.g. Moore, 1986; Horst, 1997). High frequency attenuation is caused by the tubing, the sensor separation and the time-response of the instrument itself, whilst low frequency attenuation is caused by linear detrending or block averaging.

The effect of low-pass filtering can be quantified by the use of a transfer function. Formally the transfer function H_{wc} can be written as,

$$H_{wc}(f) = \frac{C_{wc}(f)}{\overline{w'c'}} \cdot \left(\frac{C_{w\theta}(f)}{\overline{w'\theta'}}\right)^{-1}, \quad (9)$$

where C_{wc} and $C_{w\theta}$ are the cospectra of a scalar c and w, and potential temperature θ and w, respectively. $\overline{w'c'}$ and $\overline{w'\theta'}$ are 'un-attenuated' turbulent fluxes of a scalar and temperature, respectively, and f is the frequency. A commonly used approximation for the first order transfer function is (Horst, 1997)

$$H_{wc} \approx [1 + (2\pi\tau f)^2]^{-1}, \quad (10)$$

where τ is a system response time.

In this study, we determined the high frequency attenuation using a method described by Horst (1997). In the method the attenuation factor α is calculated by the equation

$$\alpha = \frac{\overline{(w'c')_a}}{\overline{w'c'}} = \frac{1}{1+\left(\frac{2\pi n_m \tau \bar{u}}{z_m - d}\right)^{\beta}}, \quad (11)$$

where z_m is the measurement height (32 m), d the zero displacement height ($d = 2/3 \times z_c$, where z_c is the canopy height, 28 m), $\bar{u}$ the mean horizontal wind speed, $\overline{(w'c')_a}$ is the attenuated flux and $\overline{w'c'}$ is the real flux. For neutral and unstable stratification $(z_m - d)/L \leq 0$, $\beta = 7/8$, $n_m = 0.085$ and for stable stratification, $(z_m - d)/L > 0$, $\beta = 1, n_m = 2.0 - 1.915/[1 + 0.5(z_m - d)/L]$.

We selected daytime (10:00-16:00 CET wintertime), unstable ($\overline{w'T'} > 0$) periods, and calculated cospectra of temperature, isoprene and water clusters for every 30 min interval. Response times of

isoprene and water clusters were then derived by using Eq. (10) and the median transfer functions (Eq. 9). After that, the flux losses were derived using the correction factor α^{-1} (Eq. 11) and the response time of the isoprene measurements, τ = 1.1 s (Fig. 3). This value is similar to that obtained by Rantala et al. (2014), who utilized disjunct EC with a PTR-QMS. The correction factor α^{-1} was finally multiplied to each VOC flux value. During daytime, the factor was mostly less than 10%, and during nighttime typically around 20%, resulting in overall correction of the isoprene flux, dominated by daytime emission, of 11%.

The value τ = 1.1 s represents the response time of the whole system including the instrument and the inlet line. Therefore, the response time should be determined for each measurement setup individually as e.g. the length of the inlet line has an effect on the attenuation (Nordbo et al., 2013 and 2014). The response time is also probably compound dependent because the attenuation of water vapor increases as a function of relative humidity (Mammarella et al., 2009). Thus, similar kind of behavior could be expected for water solvable compounds, such as methanol. In that sense, the high frequency corrections should be taken as rough estimates.

2.3.5 Flux loss due to chemical degradation

The chemical degradation of different VOCs is dependent on their concentration, reaction rates and concentrations of oxidants (O_3, NO_3, OH). Therefore the proxy for OH concentration, $[OH]_{proxy}$, was calculated according to Peräkylä et al. (2014) and Petäjä et al. (2009):

$$[OH]_{proxy} = 5.62 \times 10^5 \times UVB^{0.62} \quad (12)$$

The calculated average midday concentration of the $[OH]_{proxy}$ was $1 \cdot 10^6$ # cm^{-3}.

As the UVB radiation was not measured directly during the Bosco Fontana study, an upper limit calculation was made by using the tropospheric ultraviolet model 4.1 (TUV; Madronich 1993, Madronich and Flocke, 1999). The model was used via the link http://cprm.acd.ucar.edu/Models/TUV/Interactive_TUV/, using the Pseudo-spherical discrete ordinate 4 streams radiation transfer model and an albedo of 0.1. The NO_3 concentration was calculated as described in Peräkylä et al. (2014) from the measured concentrations of NO_2 and O_3.

The influence of chemical degradation on the measured eddy covariance fluxes depends on the relative magnitude of the chemical lifetime of the measured compound and its transport time. The transport time is the time the compound needs to get from its emission point to the actual measure point, and it can be characterized by turbulent mixing time-scale. The effect is often assessed using the Damköhler number (Damköhler, 1940), which is the ratio of the mixing time-scale to the chemical lifetime. The smaller the Damköhler number is, the less influence the chemical degradation has on

the flux. However, since both the transport time and the chemical lifetime are height dependent, a more accurate assessment of the loss is achieved by calculating the ratio of the flux at the measurement height (F) to the true surface exchange (E) e.g. using a stochastic Lagrangian transport model (Rinne et al., 2012). In Bosco Fontana, the F/E for isoprene was 0.95-0.97, indicating that the measured fluxes are between 3% and 5% lower than the emission due to the chemical degradation. For the monoterpenes (we used α-pinene), which have the lowest F/E ratio (shortest lifetime) of the measured compounds, the F/E was between 0.8 and 0.95. No corrections for the chemical degradation have been made in this study.

2.4 Modelled MVK/MACR production

After having quantified the average fraction of the isoprene flux lost between point of emission and the measurement height, this section uses an alternative method to quantify the fraction of the observed MVK/MACR flux that is expected to be produced by the atmospheric oxidation of isoprene below the measurement height. This is done by integration of the chemical kinetic equation.

The chemical destruction of isoprene F_Q, in an air column below the measurement level can be calculated as

$$F_Q = \int_0^{z_m} \sum_i k_i [R_i]\,[\mathrm{C_5H_8}]\,\mathrm{d}z, \quad (13)$$

where k_i is the rate constant, $[R_i]$ the concentration of reactant i, and $[\mathrm{C_5H_8}]$ the concentration of isoprene. The integration is done from surface to the measurement height z_m. Even though $[\mathrm{C_5H_8}]$ and $[R_i]$ are height dependent (Andronache et al., 1994, Hens et al., 2014), we assumed constant reactant and isoprene concentrations for the integration range as no profiles were measured, in order to get an order of magnitude estimate. The chemical destruction was estimated for two ranges: from the ground level 0 to the measurement height and from the notional height ($d + z_0$) to the measurement height. The angle brackets $\langle\ \rangle$ indicate that the values are constant:

$$\mathrm{Q} = \mathrm{k_i}\langle[\mathrm{R_i}]\rangle\langle[\mathrm{C_5H_8}]\rangle\mathrm{z_m} \quad (14)$$

$$\mathrm{Q} = \mathrm{k_i}\langle[\mathrm{R_i}]\rangle\langle[\mathrm{C_5H_8}]\rangle(\mathrm{z_m} - d - \mathrm{z_0}) \quad (15)$$

Due to the smaller reaction rates and the lower MVK/MACR concentration, we did not calculate the chemical destruction of MVK/MACR.

In order to estimate the yield of MVK and MACR from isoprene, we selected the isoprene chemistry mechanism from the Master Chemical Mechanism (MCM) v3.2 (Jenkin et al., 1997, Saunders et al., 2003), via website http://mcm.leeds.ac.uk/MCM/. The concentrations of MVK and MACR were calculated using the Kinetic PreProcessor (Damian et al., 2002) coupled to the box model MALTE-

BOX (Boy et al., 2013). The simulation was executed using an initial concentration of isoprene ($5.33 \cdot 10^{10}$ # cm^{-3}; measured) and constant concentrations of OH ($1 \cdot 10^{6}$ # cm^{-3}; calculated), O_3 ($2 \cdot 10^{12}$ # cm^{-3}; measured), NO ($3.5 \cdot 10^{9}$ # cm^{-3}; measured), NO_2 ($8 \cdot 10^{10}$ # cm^{-3}; measured), SO_2 ($1 \cdot 10^{9}$ # cm^{-3}; estimated) and CO ($3.5 \cdot 10^{12}$ # cm^{-3}; estimated). The temperature was further kept constant to a value of 303 K, while the start of the simulation was assumed to be at noon (local time). By dividing the initial concentration of isoprene by the summed maximum concentration of MVK and MACR, we estimate that the summed yield of MVK and MACR from oxidized isoprene is 0.35. This factor accounts for oxidation losses of MVK and MACR. A sensitivity test showed that the MVK/MACR yield response to a change in temperature and SO_2 concentration is minor. For CO, a concentration change to $5 \cdot 10^{13}$ # cm^{-3} results in a 5% lower yield. Due to the high NO_x concentration in Bosco Fontana, the reaction way via isoprene hydroxy hydroperoxides (ISOPOOH) does not form MVK/MACR.

3. Results and discussion

3.1. Comparison of procedures to identify detectable fluxes

In the following the data from 22 days of flux measurements are used by different analysis routines, and the results are compared. Negative fluxes are called downward fluxes, as it is not possible to differentiate between deposition and other sink terms such as chemical losses below the measurement height. The positive fluxes are called upward fluxes. The diurnal cycles of the fluxes derived by the classical method and automated method (evaluated using a 10 σ_{noise} threshold) are shown in Fig. 4. The signal of the remaining masses with detectable flux (between 3 and 10 σ_{noise}) quantified by the automated method is summed up and plotted as 'other'. The 24 h average fluxes of the different compounds and different methods are shown in Table 2.

The classical method identified the lower number of compounds (5), accounting for the lower total upward flux (8.53 nmol m^{-2} s^{-1}) and also the lower total downward flux (-0.28 nmol m^{-2} s^{-1}). The only compound with a flux that was deemed quantifiable by the classical method but not by the automated method with 10 σ_{noise} was $C_5H_9O_2^+$ (protonated), which contributed by 1.2% to the total downward flux and by 0.1% to the total upward flux.

The automated method with a 10 σ_{noise} threshold found eleven compounds with detectable flux and derived a total upward flux of 9.6 nmol m^{-2} s^{-1}. The downward flux reached -0.48 nmol m^{-2} s^{-1}. If the 3 σ_{noise} threshold was used, the number of compounds with detectable flux increased to 29 but the total upward flux was nearly the same (10.4 nmol m^{-2} s^{-1}) while the downward flux increased to -0.58

nmol m^{-2} s^{-1}. The main additional masses with detectable flux were acetone, acetaldehyde and acetic acid. As discussed in Sect. 2.3.2 fragments, waterclusters and isotopes identified during calibrations were removed from the data. The disregarded masses are shown in Table A1.

Figure 5 shows the diurnal variation of the net flux for the two approaches. The maximum difference in the hourly net flux between a 3 σ_{noise} threshold and a 10 σ_{noise} threshold was less than 1.3 nmol m^{-2} s^{-1} and the daily average differed less than 0.5 nmol m^{-2} s^{-1}. The major difference lies in the number of masses that are found to contribute to the total VOC flux: 29 (3 σ_{noise}), 22 (4 σ_{noise}), 22 (5 σ_{noise}), 19 (6 σ_{noise}), 15 (7 σ_{noise}), 14 (8 σ_{noise}), 12 (9 σ_{noise}), 11 (10 σ_{noise}).

The classical method is rather labor intensive, because the CCF must be checked for many different mass peaks (>150, depending on the environment where the measurements are recorded), for several different times of the campaign (overall well over 1000 CCFs). Another weakness is that the definition of a 'clear maxima' is not objective and depends on the person who is working with the data. A positive aspect is that during the manual evaluation of the data possible problems or analysis faults can be detected more easily.

Compared to the classical method, the automated method gives a fast and objective result and the quality of the fluxes can be selected by the different σ_{noise} criteria. However, using the absolute value of the signal changes the mean value of it and thereby reduces the variation and the standard deviation of the signal (see Fig. A4 and A5). For example, the standard deviation of the averaged absolute CCF was 21% smaller than the standard deviation of the averaged CCF for acetone. This effect can be seen in the difference of the mean noise in Fig. A4 and A5. The higher mean noise corrects for the lower σ_{noise}, but it is constant for different σ_{noise} criteria.

In the remaining paper, all mentioned flux values were calculated using the automated method with 3 σ_{noise} threshold and the time zone used was CET wintertime (UTC +1 h).

3.2 Comparison to other studies

Comparing VOC concentration and especially fluxes from different locations (and/or times) is challenging as the results are dependent on ecosystem type, meteorology and the surroundings of the measurement site, as well as the instrumental setup (e.g. inlet length).

The most obvious difference compared to the study by Park et al. (2013) was the number of masses showing fluxes. Park et al. (2013) found 494 (out of 664 masses) showed flux above the orange grove, whereas in this study only 29 (out of 163 masses) were found to have flux. While in both studies the results depended heavily on the σ_{noise} threshold, in this study the differences were much more subtle. In the study by Park et al. (2013), the number of ions with flux differed by two orders of magnitude.

In our study compounds which fulfilled the three 3 σ_{noise} criteria, but not the 10 σ_{noise} criteria, contributed 16% to the total downward flux, and 7% to the total upward flux. However, the amount of compounds filtered by the σ_{noise} criteria changed from 29 (3 σ_{noise}) to 11 (10 σ_{noise}).

A comparison between the measured fluxes from this study and their values at the orange grove (Park et al., 2013) can be found in Table A2. The major difference was the large upward flux of isoprene measured in Bosco Fontana, which contributed with 65% to the total net flux of 9.8 nmol m^{-2} s^{-1}. This net flux of all compounds is twice as much as at the orange orchard. All the major compounds (> 8 σ_{noise}) from the orange grove, except para-cymene, were also present in Bosco Fontana. Six of the remaining major compounds (> 8 σ_{noise}) of the orange grove had net fluxes which agree within 50% with the measured net fluxes in this study (isoprene and MVK/MACR being the exception).The net carbon exchange in Bosco Fontana is shown in Fig. 6. Isoprene is the dominating compound and contributed 77% to the carbon net flux, followed by the monoterpenes (5%), MVK/MACR (3%), methanol (3%), acetone (2%) and acetic acid (2%). Overall, the measured and identified compounds had a net carbon flux of 41.8 nmol C m^{-2} s^{-1}. Two masses were not taken into account, as their elemental composition could not be determined (Table A2).

This net flux of carbon at Bosco Fontana is about four times higher than the values published by Park et al. (2013). If the net carbon emission of the measured compounds is compared to the net uptake of CO_2 during the measurement period (2423 nmol C m^{-2} s^{-1}) the influence is less than 2 % in Bosco Fontana. The daily average value of CO_2 gas exchange was -9.2 g C m^{-2}, similar to what observed by Wilson and Baldocchi (2001) over a mixed deciduous forest.

3.3. Emission of terpenoids

The most abundant compound emitted by the Bosco Fontana forest was isoprene (protonated formula: $C_5H_9^+$), comprising over 60% of the measured total upward flux. It had a clear diurnal cycle which follows the radiation. The maximum upward flux (diurnal) at 20.6 nmol m^{-2} s^{-1} occurred just after midday. Figure 7b shows the wind rose for the isoprene flux. There are more isoprene emitting plants to the west of the site, indicated by the highest fluxes coming from this direction. Indeed, Acton et al. (2015) found that taking the contribution of the strong emitters in this wind sector into account improved the correlation between predicted and measured isoprene fluxes. Similar behavior can be seen from the wind rose of the isoprene concentrations, although the extent of the forest is smaller towards southwest, providing less opportunity for isoprene to accumulate during advection. From 21:00 to 05:00 the upward flux stayed below 0.1 nmol m^{-2} s^{-1}. The main sink of isoprene is oxidation due to reactions with OH during daytime. The calculated isoprene lifetime for daytime conditions in Bosco Fontana was 2.2 h.

The fast oxidation, together with the relatively small extent of the woodland in a mixed agricultural landscape with relatively low isoprene emissions, explains why the diurnal concentration maximum of isoprene was only 2.8 ppb, even though the isoprene upward flux was dominating all other measured VOCs. Its daily average concentration was 1.3 ppb. The emission factors of isoprene and monoterpenes in Bosco Fontana, as well as the as the relative importance of pool and *de novo* emissions, are discussed in Acton et al. (2015). Isoprene's major source globally are forests (Guenther et al., 1995), oaks are known for being isoprene emitters (Rasmussen 1970) and dominate European isoprene emissions. Potosnak et al. (2014) measured a maximum isoprene emission of 217 nmol m^{-2} s^{-1} over an oak-dominated temperate forest in central Missouri.

2-methyl-3-buten-2-ol (MBO) can dehydrate in the proton transfer reaction and form isoprene (Fall et al., 2001, de Gouw and Warneke, 2006, Kaser et al. 2013). The influence on the isoprene signal depends on the MBO concentration and the settings of the PTR-ToF. The contribution of MBO to the isoprene signal in Bosco Fontana should be minor, as the major tree species are known to be isoprene or monoterpene emitter (König et al., 1995; Harley et al., 1999; Rosenstiel et al., 2002) as confirmed by the more specific leaf level measurements of Acton et al. (2015). However, a possible MBO source could be the understory of the forest.

In Bosco Fontana, monoterpenes have been the seventh most emitted 'compound group' with a maximum diurnal upward flux of 0.7 nmol m^{-2} s^{-1}. Leaf-level measurements at Bosco Fontana presented by Acton et al. (2015) found the largest monoterpene emissions to be limonene originating from *Carpinus betulus* and *Corylus avellana* and to some extent *Comus sanguinea*, augmented with smaller emissions of α-pinene from *Q. robur* and *Acer campestre*, and β-pinene from *A. campestre* and *C. betulus*. Figure 7b shows the normalized wind rose of the monoterpenes upward flux (independent of the frequency of wind directions). The measurement site is very homogeneous, as no wind direction dependency on the monoterpenes flux was detected. This also holds for the monoterpene concentrations.

3.4. MVK/MACR and their sources

MVK and MACR have the same elemental composition (protonated formula: $C_4H_7O^+$), and cannot be separated with our instrument settings. In Bosco Fontana, 3% of the total upward VOC flux was due to MVK/MACR, which are both oxidation products of isoprene. To give an estimate of how much of the MVK/MACR flux is likely to have originated from atmospheric oxidation of isoprene below the measurement level z_m, we used two methods to estimate the flux divergence. The oxidation of isoprene is dominated by the reaction with the OH radical. The daytime maximum flux of isoprene

oxidation products between ground level and measurement height were around 0.61 nmol m^{-2} s^{-1} (Eq.14) and 0.24 nmol m^{-2} s^{-1} (Eq.15) if the lower limit is the notional height. However, the result of the integration (Eq. 13) varies considerably depending on the integration domain and the assumed profiles.

Another approach to estimate the chemical degradation is to use the look-up tables for Flux-to-Surface-Exchange (F/E) ratios created using a stochastic Lagrangian transport model by Rinne et al. (2012). For the F/E ratio we use typical daytime values of friction velocity and chemical lifetime of isoprene. Depending on the assumed oxidant profile and leaf area index, F/E ratios ranged between 0.97-0.95. Multiplying the isoprene upward flux by F/E ratio leads to the oxidation fluxes between 0.6-1.0 nmol m^{-2} s^{-1}.

According to our calculations (Sect. 2.4), 35% of the oxidized isoprene molecules will create MVK or MACR molecules (for midday conditions). The scatterplot between the measured MVK/MACR flux and the calculated source of MVK/MACR by the oxidation of isoprene below the measurement height (Fig. 8). shows a correlation coefficient of 0.81. This correlation however, does not necessarily imply causality. The biogenic VOC emissions and concentrations are light dependent, as well as the concentration of OH radicals which may lead to correlations where causality does not exist.

The hourly data in the plot was separated into day and night by using a 200 µmol m^{-2} s^{-1} photosynthetically active radiation threshold. Then the $\frac{y}{x}$ ratios of the daytime data were used to calculate the median and percentile ratios. The influence of the oxidation of isoprene to the measured MVK/MACR flux was estimated from the 25_{th} and 75_{th} percentiles ratios. If Eq. (14) was used to calculate this influence, the oxidation products of isoprene vary between 10% and 30% of the MVK/MACR flux. If Eq. (15) was used, the contribution of isoprene to the MVK/MACR flux varied between 4% and 10%.

Comparing the results of the F/E calculations with the maximum diurnal MVK/MACR flux of 1.3 nmol m^{-2} s^{-1} suggested that a contribution of 16% to 27% of the MVK/MACR flux may originate from atmospheric chemistry. Overall the oxidation of isoprene may have an important influence (4% to 30%) on the MVK/MACR flux, but fails to explain it fully.

Fluxes can also originate from direct MVK/MACR emissions from the plant as shown by Jardine et al. (2012). Other studies have shown also minor (Fares et al., 2015) or negligible (Karl et al., 2009; Karl et al., 2010) emission of MVK/MACR, however, in these studies there was a net uptake to the leaf. Part of the MVK/MACR concentration and fluxes may also be misattributed fragments from higher oxygenated hydrocarbons (Liu et al., 2013, Rivera-Rios et al., 2014). MVK and MACR have also been found to be formed from the decomposition of hydroxyl hydroperoxides (ISOPOOH) in

the PTR-MS inlet. However, the ISPOOH precursor ISOPO2 will be effectively quenched by NO. Therefore the ISOPOOH concentration in polluted environments such as the Po Valley would be expected to be very low, and consequently this artefact can be ruled out at this location. Additionally, an existing interference by ISOPOOH would most likely lead to a pretended MVK/MACR deposition, due to an expected downward flux of peroxides (Nguyen et al., 2015).

In general, a comprehensive theory of MVK/MACR emission and deposition is lacking, while in some environments (especially in the tropics) MVK/MACR are found to deposit fast, approaching the maximum rate permitted by turbulence (i.e. with a small canopy uptake resistance; cf Misztal et al., 2011, and references therein), whilst in other environments like at Bosco Fontana upward fluxes are observed.

3.5. Emission of oxygenated VOCs

The second-most emitted compound was methanol (protonated formula: CH_5O^+), whose upward flux started at 08:00, later compared with the remaining VOCs. It contributed 15% to the total upward flux (maximum at 14:30 with 4.4 nmol m^{-2} s^{-1}). Methanol is mostly emitted by plants e.g. by the plant growth metabolism (Wohlfahrt et al., 2015). From the wind rose in Fig. 7b it can be seen that the highest upward fluxes of methanol originated from the west.

The third most emitted compound was acetone, which had a diurnal maximum upward flux at 11:30 with 1.0 nmol m^{-2} s^{-1}. Its daily average contributed with over 3% to the total upward flux (daily average). It has the same elemental composition as propanal. However, the contribution of propanal to the signal is normally less than 10% (de Gouw and Warneke, 2006). Acetone sources are ubiquitous: it can be emitted from several plants and trees (Geron et al., 2002; Fall 1999), as well as from anthropogenic processes (Singh et al., 1994) or produced through secondary photochemical production (Goldstein et al., 2000).

The upward flux of acetaldehyde peaked around 11:30 at 0.7 nmol m^{-2} s^{-1}. It is a hazardous air pollutant (EPA, 1994), and plays an important role in the formation of ozone, HO_x radicals (Singh et al., 1995) and PAN (Roberts, 1990).

The maximum upward flux of acetic acid was at 11:30 at 1.0 nmol m^{-2} s^{-1}. Its sources are manifold: it is emitted by soil and vegetation, from animal husbandry, it can be produced photochemically and it is also a combustion marker for biomass and fossil fuels (Chebbi et al., 1996).

The C_6 green leaf volatiles (GLV; $C_6H_{13}O^+$) are emitted by damaged plants seconds after the damage occurred (Holopainen, 2004). They are found to be important in ‘plant communication’ and are used as ‘plant indirect defenses’ (Scala et al., 2013, and references therein). The emission of GLV

accounted 1.2% of the total emission. Similar to the monoterpenes, a fragment of GLV ($C_6H_{11}^+$; Table 2) was also measured. But unlike monoterpenes, the behavior of the parental ion and fragment are very different. While $C_6H_{13}O^+$ has a downward flux/upward flux ratio of 0.3 (Sect. 3.6), the fragment's downward flux/upward flux ratio is <1%. This leads to the assumption that the fragmentation pattern for the main GLVs measured in Bosco Fontana is different.

Ethanol participated with 1.2 % to the total upward flux. Ethanol is known to be emitted from different ecosystems, as shown in Park et al. (2013) and Kaser et al. (2013).

Other reported sources of carbonyls include conifers (e.g. Janson et al., 1999; Rinne et al., 2007) and decaying vegetation (e.g. de Gouw et al., 2000; Karl et al., 2001; Warneke et al., 2002). The remaining compounds each contributed less than 1% to the total upward flux.

3.6. VOC deposition

In case of wet or dry deposition, the ambient concentration of the deposited compound plays an important role. Figure 9 shows the total VOC concentration detected by the PTR-ToF and its diurnal behavior. The highest total VOC concentrations occur during the night, when the planetary boundary layer is shallower and the volume, into which the VOCs are emitted, is smaller. However, concentrations of biogenic VOCs (e.g. isoprene, monoterpenes) were much smaller during the night, reflecting a combination of smaller emissions and influences from air from outside the forest (the footprint for concentration measurements is much larger than the Bosco Fontana forest). By contrast, long-lived compounds, which can also be of anthropogenic origin, increase in concentration at night. One of them, methanol, showed the largest concentration and biggest downward flux (Table 3). The wind rose for the methanol concentration is shown in Fig. 7b. The largest concentrations were measured when the wind direction was northeast and southwest. The downward flux of methanol generally lasted from 01:00 to 08:00. The methanol concentration also peaked during this period, indicating that the concentrations were considerably affected by horizontal transport or secondary production. Since the largest concentrations were measured at the same time when downward fluxes were observed, the source must have been located outside of the flux footprint. Howerver, as the wind speed was below 2 m s^{-1}, a major source is probably close to the measurement site. Overall methanol accounted for 63% to the total downward flux. The main sinks of methanol are reactions with OH and dry and wet deposition, which restrict the atmospheric lifetime of methanol to nine days (Heikes et al., 2002). Heikes et al. (2002) determined the average lifetime due to the gas reactions with OH to 18 days, while the lifetime with respect to deposition was calculated to be 24 days. Applying the same procedure for Bosco Fontana results in a deposition lifetime of 280 days, which reflects the

different deposition velocities (V_d) used. For their estimate Heikes et al. (2002) used V_d = 4 mm s^{-1} while in Bosco Fontana, the average deposition velocity was an order of magnitude lower, 0.55 mm s^{-1}. As the measured downward flux is the sum of deposition and emission, just an upper limit of the deposition lifetime can be given. Additionally the ambient humidity during the campaign was on average 55%, which limits wet surfaces and thereby dry deposition. The global average also includes deposition over oceans, which is twice as fast as over land (Heikes et al., 2002).

The deposition of methanol has been observed in other studies (e.g. Holzinger et al., 2001, Goldan et al., 1995, Riemer et al., 1998, , Rantala et al., 2015, Wohlfahrt et al., 2015). Laffineur et al. (2012) observed considerable methanol uptake, which they suggest to be caused by adsorption/desorption to water films. In the bottom panel of Fig. 10, the ambient, aerodynamic and dew point temperature are shown. The colored areas in the figure mark the standard deviation of the calculated temperatures. On the onset of methanol downward flux periods(Fig. 10 upper panel), the dew temperature and aerodynamic temperature are closest to each other and the relative humidity is around 65%. The formation of dew is expected to happen during this time (01:00 to 06:00). Interestingly, the downward flux increases during the night and reaches a maximum between 07:00 and 08:00 when the relative humidity already decreased <60% and the difference between aerodynamic – and dew point temperature is around 10°C. After 08:00 the emissions dominate over the deposition and for the rest of the day the methanol flux is positive.

Acetic acid showed the second highest downward flux, which contributed with more than 16% to the total downward flux. It had also the second highest concentration (Table 3). Its lifetime is about 1.7 days in the boundary layer (Paulot et al., 2011).

With the elemental composition of $C_6H_{13}O^+$ (protonated) this C_6 green leaf volatile shows a higher downward flux (compare to its fragment $C_6H_{11}^+$), which explains 6% of the negative flux.

Ethanol had its maximum downward flux at 07:00 with -0.11 nmol m^{-2} s^{-1} and it explains 3.5 % of the total downward flux.

Next is acetone, which accounted for 1.7% to the total downward flux. It had the third highest concentration (Table 3) and the tropospheric lifetime is reported to be 15 days (Jacob et al., 2002).

An unidentified compound with the mass 73.0255 amu caused 1.6% of the total downward flux, while the remaining compounds each contributed with less than 1%.

4. Conclusions

During the Bosco Fontana campaign, up to 29 (depending on method and sigma threshold) compounds were found to have a detectable flux. The VOC exchange was dominated by isoprene

which comprised over 65% of the total net flux (on a molar basis). The high isoprene flux influenced via atmospheric oxidation the MVK/MACR flux. The calculated chemical production was able to explain up to 30% of the measured MVK/MACR flux. Thus, the major part of the MVK/MACR flux remained unaccounted and further research is needed to identify its sources.

Methanol caused over 60% of the total downward flux, which happened during the early morning. The removal was assumed to be dry deposition to water films on surfaces (incl. dew) as the downward fluxes coincided with the calculated ratios of dew point to aerodynamic temperature approaching unity. The deposition lifetime of methanol was estimated to be long compared to the global mean, which might be explained by the dry conditions at Bosco Fontana during the measurement period.

Overall, five compounds caused over 90% of the total downward flux (-0.58 nmol m^{-2} s^{-1}) and seven compounds add up to over 90% of the total upward flux (10.4 nmol m^{-2} s^{-1}). The measured VOCs contribute with less than 2% to the net exchange of carbon by CO_2.

Comparing the results with the emissions from an orange grove (Park et al., 2013), our study found far fewer compounds that showed significant exchange. The used sigma criteria (3-10) for the compound with detectable flux classification had only a minor effect on total VOC upward and downward fluxes. The largest difference in the net VOC exchange between Bosco Fontana and the orange orchard was the dominance of isoprene upward flux at Bosco Fontana, while the fluxes of other major compounds were comparable between the two measurement sites.

The classical method, which searches for CCF maxima manually, detected over 80% of the upward flux, 49% of the downward flux and 84% of the net flux, compared with the automated method, which uses a routine to find masses with flux. Thus, this study recommends the automated method, as the fast analysis, objective criteria and better flux detection are valuable assets for calculating and classifying fluxes of several hundreds of different ion peaks.

Acknowledgements

We would like to thank Markus Müller for providing the PTR-ToF Data Analyzer and Heikki Junninen and the tofTools team for providing the tofTools. We are further grateful to the Corpo Forestale dello Stato for access to the site. Thanks to all participants of the Bosco Fontana campaign, especially to Joe Acton for discussing and comparing the fluxes measured with PTR-QMS and PTR-ToF, to Ben Langford and Mhairi Coyle for helping with the installation on the tower. The data for the annual mean temperature and precipitation (UDel_AirT_Precip) was provided by the NOAA/OAR/ESRL PSD, Boulder, Colorado, USA, from their Web site at http://www.esrl.noaa.gov/psd/.

This research received funding from the EC Seventh Framework Programme (Collaborative projects "ECLAIRE", grant no. 282910, and “PEGASOS”, grant no. 265148) and from the Academy of Finland Centre of Excellence program (project number 272041).

References:

Acton, W. J. F., Schallhart, S., Langford, B., Valach, A., Rantala, P., Fares, S., Carriero, G., Tillmann, R., Tomlinson, S. J., Dragosits, U., Gianelle, D., Hewitt, C. N., and Nemitz, E.: Canopy-scale flux measurements and bottom-up emission estimates of volatile organic compounds from a mixed oak and hornbeam forest in northern Italy, Atmos. Chem. Phys. Discuss., 15, 29213-29264, doi:10.5194/acpd-15-29213-2015, 2015.

Ammann, C., Brunner, A., Spirig, C., and Neftel, A.: Technical note: Water vapour concentration and flux measurements with PTR-MS, Atmospheric Chemistry and Physics, 6, 12, 4643-4651, 2006.

Andronache, C., Chameides, W. L., Rodgers, M. O., Martinez, J., Zimmerman, P. and Greenberg, J.: Vertical distribution of isoprene in the lower boundary layer of the rural and urban southern United States, J. Geophys. Res., 99(D8), 16989–16999, doi:10.1029/94JD01027, 1994.

Baasandorj, M., Millet, D. B., Hu, L., Mitroo, D., and Williams, B. J.: Measuring acetic and formic acid by proton-transfer-reaction mass spectrometry: sensitivity, humidity dependence, and quantifying interferences, Atmos. Meas. Tech., 8, 1303-1321, doi:10.5194/amt-8-1303-2015, 2015.

Bloss, C., Wagner, V., Bonzanini, A., Jenkin, M.E., Wirtz, K., Martin-Reviejo, M. and Pilling, M.J.: Evaluation of detailed aromatic mechanisms (MCMv3 and MCMv3.1) against environmental chamber data, Atmospheric Chemistry and Physics 5, 623–639, 2005.

Boy, M., Mogensen, D., Smolander, S., Zhou, L., Nieminen, T., Paasonen, P., Plass-Dülmer, C., Sipilä, M., Petäjä, T., Mauldin, L., Berresheim, H., and Kulmala, M.: Oxidation of SO2 by stabilized Criegee Intermediate (sCI) radicals as a crucial source for atmospheric sulphuric acid concentrations, Atmos. Chem. Phys., 13:3865–3879, 2013.

Businger, J. A., and Oncley, S. P.: Flux measurement with conditional sampling, J. Atmos. Ocean. Tech., 7, 349-352, 1990.

Chebbi, A. and Carlier, P.: Carboxylic acids in the troposphere, occurrence, sources, and sinks: A review, Atmospheric Environment, Volume 30, Issue 24, 4233-4249, ISSN 1352-2310, http://dx.doi.org/10.1016/1352-2310(96)00102-1, 1996.

Dalponte, M., Bruzzone, L. and Gianelle, D.: Fusion of hyperspectral and LIDAR remote sensing data for classification of complex forest areas, Geoscience and Remote Sensing, 46, 5, 1416-1427, 2008.

Damian, V., Sandu, A., Damian, M., Potra, F. and Carmichael, G. R. The kinetic preprocessor KPP – a software environment for solving chemical kinetics, Comput. Chem. Eng., 26:1567–1579, 2002.

Damköhler, G.: Der Einfluss der Turbulenz auf die Flammengeschwindigkeit in Gasgemischen, Zeitschrift für Electrochemie und Angewandte Physikalische Chemie, 46, 601–626, 1940.

de Gouw, J. A. and Warneke, C.: Measurements of volatile organic compounds in the earth's atmosphere using proton-transfer-reaction mass spectrometry, Mass Spectrom. Rev., 26: 223–257. doi: 10.1002/mas.20119, 2006.

de Gouw, J. A., Howard, C. J., Custer, T. G., Baker, B. M. and Fall, R.: Proton-transfer chemical-ionization mass spectrometry allows real-time analysis of volatile organic compounds released from cutting and drying of crops, Environmental science & technology, 34, 12, 2640-2648, 2000.

Dolman, A. J.: Estimates of roughness length and zero plane displacement for a foliated and non-foliated oak canopy, Agricultural and Forest Meteorology, 36, 241-248, 1986.

Derwent, R. G., Jenkin, M. E., Saunders, S. M., Pilling, M. J., Simmonds, P. G., Passant, N. R., Dollard, G. J., Dumitrean, P. and Kent, A.: Photochemical ozone formation in north west Europe and its control, Atmos. Environ, 37, 1983–1991, 2003.

EPA: Chemical Summary for Acetaldehyde, EPA 749-F-94-003a, Office of Pollution Prevention and Toxics, available at: http://onlinelibrary.wiley.com/doi/10.1002/9781118747926.app1/pdf (last access: 13 October 2015), 1994.

Fall, R.: Reactive hydrocarbons in the atmosphere, Academic Press, San Diego 41-96, 1999.

Fall, R., Karl, T., Jordan, A. and Lindinger, W.: Biogenic C5 VOCs: release from leaves after freeze–thaw wounding and occurrence in air at a high mountain observatory, Atmospheric Environment, 35, 22,3905 – 3916, 2001.

Fares, S., Paoletti, E., Loreto, F., and Brilli, F.: Bidirectional Flux of Methyl Vinyl Ketone and Methacrolein in Trees with Different Isoprenoid Emission under Realistic Ambient Concentrations, Environ Sci Technol, 49, 7735-7742, doi: 10.1021/acs.est.5b00673, 2015.

Fehsenfeld, F., Calvert, J., Fall, R., Goldan, P., Guenther, A. B., Hewitt, C.N., Lamb, B., Liu, S., Trainer, M., Westberg, H. and Zimmerman, P.: Emissions of volatile organic compounds from vegetation and the implications for atmospheric chemistry, Global Biogeochem. Cycles, 6(4), 389–430, 1992.

Foken, T. and Wichura, B.: Tools for quality assessment of surface-based flux measurements, Agricultural and Forest Meteorology 78: 83–105, 1996.

Fuentes, J. D., Wang, D., Neumann, H. H., Gillespie, T. J., Den Hartog, G. and Dann, T. F.: Ambient biogenic hydrocarbons and isoprene emissions from a mixed deciduous forest. J. Atmos. Chem., 25, 67-95, 1996.

Fuentes, J. D., Gu, L., Lerdau, M., Atkinson, R., Baldocchi, D., Bottenheim, J. W., Ciccioli, P., Lamb, B., Geron, C., Guenther, A. B., Sharkey, T. D. and Stockwell W.: Biogenic Hydrocarbons in the Atmospheric Boundary Layer: A Review, Bull. Amer. Meteor. Soc., 81, 1537–1575, 2000.

Garland, J. A.: Dry Deposition of Sulfur-Dioxide to Land and Water Surfaces, P. Roy. Soc. A-Math. Phy., 354, 245–268, 1977.

Geron, C., Guenther, A. B., Greenberg, J., Loescher, H. W., Clark, D. and Baker, B.: Biogenic volatile organic compound emissions from a lowland tropical wet forest in Costa Rica, Atmospheric Environment, Volume 36, Issue 23, 3793-3802, ISSN 1352-2310, 2002.

Goldan, P. D., Kuster, W. C., Fehsenfeld, F. C. and Montzka, S. A.: Hydrocarbon measurements in the southeastern United States: The Rural Oxidants in the Southern Environment (ROSE) Program 1990, J. Geophys. Res., 100(D12), 25945–25963, doi:10.1029/95JD02607, 1995.

Goldstein, A. and Schade, G. W.: Quantifying biogenic and anthropogenic contributions to acetone mixing ratios in a rural environment, Atmospheric Environment, Volume 34, Issues 29–30, 4997-5006, ISSN 1352-2310, 2000.

Graus, M., Müller, M., and Hansel, A.: High resolution PTR-TOF: quantification and formula confirmation of VOC in real time, J. Am. Soc. Mass Spectr., 21, 1037–1044, 2010.

Guenther, A. B., Hewitt, C. N., Erickson, D., Fall, R., Geron, C., Graedel, T., Harley, P., Klinger, L., Lerdau, M., McKay, W. A., Pierce, T., Scholes, B., Steinbrecher, R., Tallamraju, R., Taylor, J., and Zimmerman, P., A global model of natural volatile organic compound emissions. J. Geophys. Res., 100(D5), 8873–8892, doi:10.1029/94JD02950, 1995.

Guenther, A. B., Greenberg, J., Harley, P., Helmig, D., Klinger, L., Vierling, L., Zimmerman, P. and Geron, C.: Leaf, branch, stand and landscape scale measurements of volatile organic compound fluxes from U.S. woodlands, Tree Physiol 16, 1-2, 17-24 doi:10.1093/treephys/16.1-2.17, 1996.

Guenther, A. B., Jiang, X., Heald, C. L., Sakulyanontvittaya, T., Duhl, T., Emmons, L. K. and Wang, X.: The Model of Emissions of Gases and Aerosols from Nature version 2.1 (MEGAN2.1): an extended and updated framework for modeling biogenic emissions, Geosci. Model Dev., 5, 1471-1492, doi:10.5194/gmd-5-1471-2012, 2012.

Harley, P. C., Monson, R. K., and Lerdau, M. T.: Ecological and evolutionary aspects of isoprene emission from plants, Oecologia, 118, 2, 109-123, 1999.

Heikes, B.G., Chang, W.N , Pilson, M.E.Q., Swift, E., Singh, H.B., Guenther, A., Jacob, D.J.,. Field, B.D, Fall, R., Riemer, D. and Brand, L.: Atmospheric methanol budget and ocean implication, Global Biogeochemical Cycles, 16, 1133, 2002.

Hens, K., Novelli, A., Martinez, M., Auld, J., Axinte, R., Bohn, B., Fischer, H., Keronen, P., Kubistin, D., Nölscher, A. C., Oswald, R., Paasonen, P., Petäjä, T., Regelin, E., Sander, R., Sinha, V., Sipilä, M., Taraborrelli, D., Tatum Ernest, C., Williams, J., Lelieveld, J., and Harder, H.: Observation and modelling of HOx radicals in a boreal forest, Atmos. Chem. Phys., 14, 8723-8747, doi:10.5194/acp-14-8723-2014, 2014.

Herbig, J., Müller, M., Schallhart, S., Titzmann, T., Graus, M., and Hansel, A.: On-line breath analysis with PTR-TOF, Journal of Breath Research, 3, 027004, doi:10.1088/1752- 7155/3/2/027004, 2009.

Holopainen, J. K.: Multiple functions of inducible plant volatiles, Trends in plant science9, 11, 529-533, 2004.

Holzinger, R., Jordan, A., Hansel, A. and Lindinger W.: Methanol measurements in the lower troposphere near Innsbruck (047°16′N; 011°24′E), Austria, Atmospheric Environment, 35, 14, 2525-2532, 2001.

Horst, T. W.: A simple formula for attenuation of eddy fluxes measured with first-order-response scalar sensors, Boundary-Layer Meteorology 82: 219–233, 1997.

Jacob, D. J., Field, B. D., Jin, E. M., Bey, I., Li, Q., Logan, J. A., Yantosca, R. M., and Singh, H. B.: Atmospheric budget of acetone, J. Geophys. Res.-Atmos., 107, 4100, doi:10.1029/2001JD000694, 2002.

Janson, R., and De Serves, C. and Romero, R.: Emission of isoprene and carbonyl compounds from a boreal forest and wetland in Sweden, Agricultural and Forest Meteorology, 98, 671-681, 1999.

Jardine, K. J., Monson, R. K., Abrell, L., Saleska, S. R., Arneth, A., Jardine, A., Ishida, F. Y., Serrano, A. M. Y., Artaxo, P., Karl, T., Fares, S., Goldstein, A., Loreto, F. and Huxman, T.: Within-plant isoprene oxidation confirmed by direct emissions of oxidation products methyl vinyl ketone and methacrolein, Global Change Biology, 18: 973–984. doi: 10.1111/j.1365-2486.2011.02610.x, 2012.

Jenkin, M. E., Saunders, S. M., and Pilling, M. J.: The tropospheric degradation of volatile organic compounds: A protocol for mechanism development, Atmos. Environ., 31:81–104, 1997.

Jordan, A., Haidacher, S., Hanel, G., Hartungen, E., Märk, L., Seehauser, H., Schottkowsky, R., Sulzer, P., and Märk, T. D.: A high resolution and high sensitivity proton-transfer-reaction time-of-flight mass spectrometer (PTR-TOF-MS), Int. J. Mass Spectrom., 286, 122–128, 2009.

Junninen, H., Ehn, M., Petäjä, T., Luosujärvi, L., Kotiaho, T., Kostiainen, R., Rohner, U., Gonin, M., Fuhrer, K., Kulmala, M. and Worsnop, D. R.: A high-resolution mass spectrometer to measure atmospheric ion composition, Atmospheric Measurement Techniques, 3, 4, 1039-1053, 2010.

Kaimal, J. C. and Finnigan, J. J.: Atmospheric Boundary Layer Flows: Their Structure and Measurement, Oxford University press, New York, USA, 1994.

Karl, T., Guenther, A. B., Jordan, A., Fall, R. and Lindinger, W.: Eddy covariance measurement of biogenic oxygenated VOC emissions from hay harvesting, Atmospheric Environment, 35, 491–495, doi:10.1016/S1352-2310(00)00405-2, Volume 35, Issue 3, 2001.

Karl, T. G., Spirig, C., Rinne, J., Stroud, C., Prevost, P., Greenberg, J., Fall, R., and Guenther, A.: Virtual disjunct eddy covariance measurements of organic compound fluxes from a subalpine forest using proton transfer reaction mass spectrometry, Atmos. Chem. Phys., 2, 279-291, doi:10.5194/acp-2-279-2002, 2002.

Karl, T., Guenther, A., Turnipseed, A., Tyndall, G., Artaxo, P., and Martin, S.: Rapid formation of isoprene photo-oxidation products observed in Amazonia, Atmos. Chem. Phys., 9, 7753-7767, 2009.

Karl, T., Harley, P., Emmons, L., Thornton, B., Guenther, A., Basu, C., Turnipseed, A., and Jardine, K.: Efficient Atmospheric Cleansing of Oxidized Organic Trace Gases by Vegetation, Science, 330, 816 - 819, doi: 10.1126/science.1192534, 2010.

Kaser, L., Karl, T., Guenther, A. B., Graus, M., Schnitzhofer, R., Turnipseed, A., Fischer, L., Harley, P., Madronich, M., Gochis, D., Keutsch, F. N., and Hansel, A.: Undisturbed and disturbed

above canopy ponderosa pine emissions: PTR-TOF-MS measurements and MEGAN 2.1 model results, Atmos. Chem. Phys., 13, 11935-11947, doi:10.5194/acp-13-11935-2013, 2013.

Kesselmeier, J. and Staudt, M.: Biogenic volatile organic compounds (VOC): an overview on emission, physiology and ecology, Journal of Atmospheric Chemistry, 33, 1, 23-88, 1999.

König, G., Brunda, M., Puxbaum, H., Hewitt, C. N., Duckham, S. C. and Rudolph, J.: Relative contribution of oxygenated hydrocarbons to the total biogenic VOC emissions of selected mid-European agricultural and natural plant species. Atmospheric Environment, 29, 8, 861-874, 1995.

Kulmala M., Toivonen A., Mäkelä J. and Laaksonen A.: Analysis of the growth of nucleation mode particles observed in boreal forest, Tellus 50B: 449–462, 1998.

Laffineur, Q., Aubinet, M., Schoon, N., Amelynck, C., Müller, J.-F., Dewulf, J., Van Langenhove, H., Steppe, K., and Heinesch, B.: Abiotic and biotic control of methanol exchanges in a temperate mixed forest, Atmos. Chem. Phys., 12, 577-590, doi:10.5194/acp-12-577-2012, 2012.

Lamb, B., Westberg, H. and Allwine, G.: Biogenic hydrocarbon emissions from decidous and coniferous trees in the United States, J. geophys. Res., 90 (D1), 2380–2390, 1985.

Langford, B., Acton, W., Ammann, C., Valach, A., Nemitz E.: Eddy-covariance data with low signal-to-noise ratio: time-lag determination, uncertainties and limit of detection. Atmos. Meas. Tech. Discuss., 8, 2913-2955, 2015

Lawrence M. G: The Relationship between Relative Humidity and the Dewpoint Temperature in Moist Air: A Simple Conversion and Applications, Bull. Amer. Meteor. Soc., 86, 225–233, doi: http://dx.doi.org/10.1175/BAMS-86-2-225, 2005.

Lee, X., Massman, W., and Law, B.: Handbook of Micrometeorology: A Guide for Surface Flux Measurements and Analysis, Kluwer Academic Publisher, Dordrecht, 2004.

Liu, Y. J., Herdlinger-Blatt, I., McKinney, K. A. and Martin, S. T.: Production of methyl vinyl ketone and methacrolein via the hydroperoxyl pathway of isoprene oxidation, Atmospheric Chemistry and Physics,13, 11,5715--5730, 2013.

Madronich, S.: UV radiation in the natural and perturbed atmosphere, in Environmental Effects of UV (Ultraviolet) Radiation, 17-69, CRC Press, Boca Raton, 1993.

Madronich, S. and Flocke, S.: The role of solar radiation in atmospheric chemistry, The Handbook of Environmental Chemistry, Vol. 2. Springer, Berlin, 1-26, 1999.

Mammarella, I., Launiainen, S., Gronholm, T., Keronen, P., Pumpanen, J., Rannik, Ü., and Vesala, T.: Relative humidity effect on the high-frequency attenuation of water vapor flux measured by a closed-path eddy covariance system, Journal of Atmospheric and Oceanic Technology, 26, 9, 1856-1866, 2009.

Misztal, P. K., Nemitz, E., Langford, B., Di Marco, C. F., Phillips, G. J., Hewitt, C. N., MacKenzie, A. R., Owen, S. M., Fowler, D., Heal, M. R., and Cape, J. N.: Direct ecosystem fluxes of volatile organic compounds from oil palms in South-East Asia, Atmos. Chem. Phys., 11, 8995-9017, doi:10.5194/acp-11-8995-2011, 2011.

Mogensen, D., Gierens, R., Crowley, J. N., Keronen, P., Smolander, S., Sogachev, A., Nölscher, A. C., Zhou, L., Kulmala, M., Tang, M. J., Williams, J., and Boy, M.: Simulations of atmospheric OH, O3 and NO3 reactivities within and above the boreal forest, Atmos. Chem. Phys., 15, 3909-3932, doi:10.5194/acp-15-3909-2015, 2015.

Monks, P. S., Granier, C., Fuzzi, S., Stohl, A.,Williams, M. L., Akimoto, H., Amann, M., Baklanov, A., Baltensperger, U., Bey, I., Blake, N., Blake, R. S., Carslaw, K., Cooper, O. R., Dentener, F., Fowler, D., Fragkou, E., Frost, G. J., Generoso, S., Ginoux, P., Grewe, V., Guenther, A., Hansson, H. C., Henne, S., Hjorth, J., Hofzumahaus, A., Huntrieser, H., Isaksen, I. S. A., Jenkin, M. E., Kaiser, J., Kanakidou, M., Klimont, Z., Kulmala, M., Laj, P., Lawrence, M. G., Lee, J. D., Liousse, C., Maione, M., McFiggans, G., Metzger, A., Mieville, A., Moussiopoulos, N., Orlando, J. J., O'Dowd, C. D., Palmer, P. I., Parrish, D. D., Petzold, A., Platt, U., Pöschl, U., Prévôt, A. S. H., Reeves, C. E., Reimann, S., Rudich, Y., Sellegri, K., Steinbrecher, R., Simpson, D., ten Brink, H., Theloke, J., van derWerf, G. R., Vautard, R., Vestreng, V., Vlachokostas, C., and von Glasow, R.: Atmospheric composition change – global and regional air quality, Atmos. Environ., 43, 5268–5350, doi:10.1016/j.atmosenv.2009.08.021, 2009.

Moore, C. J.: Frequency response corrections for eddy correlation systems, Boundary-Layer Meteorology, 37, 17–35, 1986.

Müller, M., Graus, M., Ruuskanen, T. M., Schnitzhofer, R., Bamberger, I., Kaser, L., Titzmann, T., Hörtnagl, L., Wohlfahrt, G., Karl, T., and Hansel, A.: First eddy covariance flux measurements by PTR-TOF, Atmos. Meas. Tech., 3, 387-395, doi:10.5194/amt-3-387-2010, 2010.

Müller, M., Mikoviny, T., Jud, W., D'Anna, B. and Wisthaler, A.: A new software tool for the analysis of high resolution PTR-TOF mass spectra, Chemometrics and Intelligent Laboratory Systems, 127, 158-165, 2013.

Naik, V., Fiore, A. M., Horowitz, L. W., Singh, H. B., Wiedinmyer, C., Guenther, A., de Gouw, J. A., Millet, D. B., Goldan, P. D., Kuster, W. C., and Goldstein, A.: Observational constraints on the global atmospheric budget of ethanol, Atmos. Chem. Phys., 10, 5361-5370, doi:10.5194/acp-10-5361-2010, 2010.

Nemitz, E., Hargreaves, K. J., Neftel, A., Loubet, B., Cellier, P., Dorsey, J. R., Flynn, M., Hensen, A., Weidinger, T., Meszaros, R., Horvath, L., Dämmgen, U., Frühauf, C., Löpmeier, F. J., Gallagher, M. W., and Sutton, M. A.: Intercomparison and assessment of turbulent and physiological exchange parameters of grassland, Biogeosciences, 6, 1445-1466, doi:10.5194/bg-6-1445-2009, 2009.

Nguyen, T. B., Crounse, J. D., Teng, A. P., St. Clair, J. M., Paulot, F., Wolfe, G. M., and Wennberg, P. O.: Rapid deposition of oxidized biogenic compounds to a temperate forest, P. Nat. Acad. Sci. USA, 112, E392-E401, doi: 10.1073/pnas.1418702112, 2015.

Nordbo, A., Kekäläinen, P., Siivola, E., Lehto, R., Vesala, T., and Timonen, J.: Tube transport of water vapor with condensation and desorption, Applied Physics Letters, 102, 2013.

Nordbo, A., Kekäläinen, P., Siivola, E., Mammarella, I., Timonen, J., and Vesala, T.: Sorption-Caused Attenuation and Delay of Water Vapor Signals in Eddy-Covariance Sampling Tubes and Filters, Journal of Atmospheric and Oceanic Technology, 31, 2629–2649, 2014.

Owen, P. R. and Thompson, W. R.: Heat transfer across rough surfaces, J. Fluid Mech., 15, 321–334, 1963.

Paasonen, P., Asmi, A., Petäjä, T., Kajos, M. K., Äijälä, M., Junninen, H., Holst, T., Abbatt, J. P. D., Arneth, A., Birmili, W., van der Gon, H. D., Hamed, A., Hoffer, A., Laakso, L., Laaksonen, A., Leaitch, W. R., Plass-Dülmer, C., Pryor, S. C., Räisänen, P., Swietlicki, E., Wiedensohler, A., Worsnop, D. R., Kerminen, V.-M. and Kulmala, M.: Warming induced increase in aerosol number concentration likely to moderate climate change, Nature Geosci. 6: 438–442, 2013.

Park, J.-H., Goldstein, A. H., Timkovsky, J., Fares, S., Weber, R., Karlik, J. and Holzinger R.: Active Atmosphere-Ecosystem Exchange of the Vast Majority of Detected Volatile Organic Compounds, Science, 9, 341 (6146), 643-647.doi:10.1126/science.1235053, 2013.

Paulot, F., Wunch, D., Crounse, J. D., Toon, G. C., Millet, D. B., DeCarlo, P. F., Vigouroux, C., Deutscher, N. M., González Abad, G., Notholt, J., Warneke, T., Hannigan, J. W., Warneke, C., de Gouw, J. A., Dunlea, E. J., De Maziére, M., Griffith, D. W. T., Bernath, P., Jimenez, J. L. and Wennberg, P. O.: Importance of secondary sources in the atmospheric budgets of formic and acetic acids, Atmospheric Chemistry and Physics, 11, 2011.

Peräkylä, O., Vogt, M., Tikkanen, O.-P., Laurila, T., Kajos, M. K., Rantala, P. A., Patokoski, J., Aalto, J., Yli-Juuti, T., Ehn, M., Sipilä, M., Paasonen, P., Rissanen, M., Nieminen, T., Taipale, R., Keronen, P., Lappalainen, H. K., Ruuskanen, T. M., Rinne, J., Kerminen, V.-M., Kulmala, M., Bäck, J. and Petäjä, T.: Monoterpenes' oxidation capacity and rate over a boreal forest: temporal variation and connection to growth of newly formed particles, Boreal Env. Res. 19 supp. B, 293-310, 2014.

Petäjä, T., Mauldin, R. L. III, Kosciuch, E., McGrath J., Nieminen, T., Paasonen, P., Boy, M., Adamov, A., Kotiaho, T. and Kulmala, M.: Sulfuric acid and OH concentrations in a boreal forest site, Atmos. Chem. Phys. 9: 7435–7448, 2009.

Potosnak, M. J., LeStourgeon, L., Pallardy, S. G., Hosman, K. P., Gu, L., Karl, T., Geron, C. and Guenther, A. B.: Observed and modeled ecosystem isoprene fluxes from an oak-dominated temperate forest and the influence of drought stress, Atmospheric Environment, 84, 314-322, 2014.

Rannik, Ü.: On the surface layer similarity at a complex forest site, J. Geophys. Res., 103(D8), 8685–8697, doi:10.1029/98JD00086, 1998.

Rantala, P., Taipale, R., Aalto, J., Kajos, M. K., Patokoski, J., Ruuskanen, T. M. and Rinne, J.: Continuous flux measurements of VOCs using PTR-MS — reliability and feasibility of disjunct-eddy-covariance, surface-layer-gradient, and surface-layer-profile methods, Boreal Env. Res. 19 (suppl. B): 87–107, 2014.

Rantala, P., Aalto, J., Taipale, R., Ruuskanen, T. M., and Rinne, J.: Annual cycle of volatile organic compound exchange between a boreal pine forest and the atmosphere, Biogeosciences, 12, 5753–5770, 2015.

Rasmussen, R. A.: Isoprene: identified as a forest-type emission to the atmosphere, Environ. Sci. Technol., 4 (8), pp 667–671, 1970.

Riemer, D., Pos, W., Milne, P., Farmer, C., Zika, R., Apel, E., Olszyna, K., Kliendienst, T., Lonneman, W., Bertman, S., Shepson, P. and Starn, T.: Observations of nonmethane hydrocarbons

and oxygenated volatile organic compounds at a rural site in the southeastern United States, Journal of Geophysical Research: Atmospheres, 103, D21, 28111-28128, 1998.

Riipinen, I., Yli-Juuti, T., Pierce, J. R., Petäjä, T.,Worsnop, D. R., Kulmala, M. and Donahue, N. M.: The contribution of organics to atmospheric nanoparticle growth, Nature Geosci. 5: 453–458, 2012.

Rinne, J. and Ammann, C.: Disjunct eddy covariance method, in: Eddy Covariance Handbook, edited by: Aubinet, M., Vesala, T., and Papale, D., Springer, New York, USA, ISBN 978-94-007-2350-4, e-ISBN 978-94-007-2351-1, doi:10.1007/978-94-007-2351-1, 291–307, 2012.

Rinne, J., Guenther, A. B., Warneke, C., de Gouw, J. A., Luxembourg, S. L.: Disjunct eddy covariance technique for trace gas flux measurements, Geophys. Res. Lett., 28, 3139–3142, 2001.

Rinne, J., Taipale, R., Markkanen, T., Ruuskanen, T. M., Hellén, H., Kajos, M. K., Vesala, T., and Kulmala, M.: Hydrocarbon fluxes above a Scots pine forest canopy: measurements and modeling, Atmos. Chem. Phys., 7, 3361-3372, doi:10.5194/acp-7-3361-2007, 2007.

Rinne, J., Markkanen, T., Ruuskanen, T. M., Petäjä, T., Keronen, P., Tang, M. J., Crowley, J. N., Rannik, Ü., and Vesala, T.: Effect of chemical degradation on fluxes of reactive compounds – a study with a stochastic Lagrangian transport model, Atmos. Chem. Phys., 12, 4843-4854, doi:10.5194/acp-12-4843-2012, 2012.

Rivera-Rios, J. C., Nguyen, T. B., Crounse, J. D., Jud, W. St. Clair, J. M., Mikoviny, T., Gilman, J. B., Lerner, B. M., Kaiser, J. B., de Gouw, J., Wisthaler, A., Hansel, A., Wennberg P. O., Seinfeld, J. H. and Keutsch, F. N.: Conversion of hydroperoxides to carbonyls in field and laboratory instrumentation: Observational bias in diagnosing pristine versus anthropogenically controlled atmospheric chemistry, Geophys. Res. Lett., 41, 8645–8651, doi:10.1002/2014GL061919, 2014.

Roberts, J. M.: The atmospheric chemistry of organic nitrates, Atmos. Environ., 24A, 243–287, 1990.

Rosenstiel, T. N., Fisher, A. J., Fall, R. and Monson, R. K.: Differential accumulation of dimethylallyl diphosphate in leaves and needles of isoprene-and methylbutenol-emitting and nonemitting species, Plant Physiology, 129, 3, 1276-1284, 2002.

Ruuskanen, T. M., Müller, M., Schnitzhofer, R., Karl, T., Graus, M., Bamberger, I., Hörtnagl, L., Brilli, F., Wohlfahrt, G., and Hansel, A.: Eddy covariance VOC emission and deposition fluxes above grassland using PTR-TOF, Atmos. Chem. Phys., 11, 611-625, doi:10.5194/acp-11-611-2011, 2011.

Saunders, S. M., Jenkin, M. E., Derwent, R. G., and Pilling, M. J.: Protocol for the development of the Master Chemical Mechanism, MCM v3 (Part A): tropospheric degradation of nonaromatic volatile organic compounds, Atmos. Chem. Phys., 3:161–180, 2003.

Scala, A., Allmann, S., Mirabella, R., Haring, M. A., and Schuurink, R. C.: Green leaf volatiles: a plant's multifunctional weapon against herbivores and pathogens, International journal of molecular sciences, 14, 9, 17781-17811, 2013.

Singh, H. B., O'Hara, D., Herlth, D., Sachse, W., Blake, D. R., Bradshaw, J. D., Kanakidou, M. and Crutzen P. J.: Acetone in the atmosphere: Distribution, sources, and sinks, J. Geophys. Res., 99(D1), 1805–1819, doi:10.1029/93JD00764, 1994.

Singh, H. B., Kanakidou, M., Crutzen, P. J. and Jacob, D. J.: High concentrations and photochemical fate of oxygenated hydrocarbons in the global troposphere, Nature, 378, 50–54, 1995.

Taipale, R., Ruuskanen, T. M. and Rinne J.: Lag time determination in DEC measurements with PTR-MS. Atmospheric Measurement Techniques 3: 405–429 , 2010.

Tunved, P., Hansson, H.-C., Kerminen, V.-M., Ström, J., Dal Maso, M., Lihavainen, H., Viisanen, Y., Aalto, P. P., Komppula, M. and Kulmala, M.: High natural aerosol loading over boreal forests, Science, 312, 5771, 261-263, 2006.

Vickers D. and Mahrt, L.: Quality Control and Flux Sampling Problems for Tower and Aircraft Data, J. Atmos. Oceanic Technol., 14, 512–526, 1997.

Warneke, C., Luxembourg, S. L., de Gouw, J. A., Rinne, J., Guenther, A. B. and Fall, R.: Disjunct eddy covariance measurements of oxygenated volatile organic compounds fluxes from an alfalfa field before and after cutting, J. Geophys. Res., 107(D8), D8, ACH-6, doi:10.1029/2001JD000594, 2002.

Webb, E. K., Pearman, G. I., and Leuning, R.: Correction of flux measurements for density effects due to heat and water vapour transfer, Q. J. Roy. Meteor. Soc., 106, 85–100, 1980.

Willmott, C. J. and Matsuura, K.: Terrestrial Air Temperature: 1900-2010 Gridded Monthly Time Series (Version 3.01), http://climate.geog.udel.edu/~climate/html_pages/Global2011/README.GlobalTsT2011.html, access date: 21.08.2015, 2012a.

Willmott, C. J. and Matsuura, K.: Terrestrial Precipitation: 1900-2010 Gridded Monthly Time Series (Version 3.01),

http://climate.geog.udel.edu/~climate/html_pages/Global2011/README.GlobalTsP2011.html, access date: 21.08.2015, 2012b.

Wilson K.B. and Baldocchi D.D.: Comparing independent estimates of carbon dioxide exchange over 5 years at a deciduous forest in the southeastern United States, journal of geophysical research, 106, 167–34, 2001.

Wohlfahrt, G., Amelynck, C., Ammann, C., Arneth, A., Bamberger, I., Goldstein, A. H., Gu, L., Guenther, A., Hansel, A., Heinesch, B., Holst, T., Hörtnagl, L., Karl, T., Laffineur, Q., Neftel, A., McKinney, K., Munger, J. W., Pallardy, S. G., Schade, G. W., Seco, R., and Schoon, N.: An ecosystem-scale perspective of the net land methanol flux: synthesis of micrometeorological flux measurements, Atmos. Chem. Phys. Discuss., 15, 2577-2613, doi:10.5194/acpd-15-2577-2015, 2015.

Table 1: Comparison between the classical and the automated method for calculating VOC fluxes.

Step	Classical	Automated
	‘compound with exchange' detection:	
CCF data used	30 min	203·30 min
CCF preparation	none	average; absolute
amount of CCFs checked per compound	>20	1
detection of significant flux	manual	automated
threshold dependent results	no	yes
Maximum of found masses in literature [1]	10-20	ca. 500
	flux data calculation:	
Lag time calculation	variable	constant; 2.6 s
CCF used for lag time	30 min smoothed	203·30 min
Wind vector rotation	2-d	
QC: vertical rotation	5°	
QC: Stationary criteria	70%	
fluxes calculated from	30 min CCFs	

[1] The amount of compounds with exchange is dependent on many side specific factors (e.g. ecosystem, meteorological characteristics)

Table 2: Downward flux (df) and upward flux (uf) calculated with different methods. The individual compounds listed under automated are for a 10 σ_{noise} threshold, the remaining compounds (between 3 and 10 σ_{noise}) are summed up onder 'other'

possible compound	mass (prot.) Th	elemental composition	classical method		automated method	
			% of total downward flux (df) or upward flux (uf)			
			df (-0.28)*	uf (8.5)*	df (-0.58)*	uf (10.4)*
isoprene[c]	69.0699	$C_5H_9^+$	0.2	75.0	0.0	62.4
methanol[c]	33.0335	$C_1H_5O_1^+$	97.3	18.4	63.2	14.8
acetone[c]	59.0491	$C_3H_7O_1^+$			1.7	3.3
MVK/MACR[c]	71.0491	$C_4H_7O_1^+$	1.1	3.9	0.8	3.0
acetaldehyde[c]	45.0335	$C_2H_5O_1^+$			0.2	2.2
monoterpenes[c]	137.133	$C_{10}H_{17}^+$	0.2	2.6	0.1	2.1
acetic acid[1]	61.0284	$C_2H_5O_2^+$			16.7	3.0
acrolein[c]	57.0335	$C_3H_5O_1^+$			0.3	0.8
hydroxyacetone	75.0441	$C_3H_7O_2^+$			0.8	0.7
C_8 GLV[2]	83.0855	$C_6H_{11}^+$			0.0	0.3
pentanal	85.0648	$C_5H_9O_1^+$			0.1	0.2
unknown	101.0597	$C_5H_9O_2^+$	1.2	0.1	0	0
other (18)					16.2	7.0

* shows the total uF or dF in nmol m^{-2} s^{-1};

[1] acetic acid was corrected for fragmentation (see Sect. 2.3.2)

[2] C_6 green leaf volatiles (GLV) are calculated via the fragment $C_6H_{11}^+$;
the fragmentation pattern and the sensitivity of hexanal were used.

Table 3: Compounds with downward flux, their daily averaged: concentration, downward flux, deposition velocity and their respective lifetimes.

compound	concentration [ppb]	downward flux [nmol m^{-2} s^{-1}]	lifetime [days]	Deposition velocity [mm s^{-1}]
methanol	14.3	0.36	9[a]	0.56
acetic acid	4.9	0.10	1.7[b]	0.50
C_6 GLV ($C_6H_{13}O_1^+$)	0.8	0.04	-	0.15
ethanol	0.6	0.02	2.8[c]	0.55
acetone	4.7	0.01	15[d]	0.05
73.0255	0.2	0.01	-	1.4

[a] atmospheric lifetime according to Heikes et al. (2002)
[b] lifetime in the boundary layer according to Paulot et al. (2011)
[c] atmospheric lifetime according to Naik et al. (2010)
[d] tropospheric lifetime according to Jacob et al. (2002)

Figure 1: Satellite picture (Imagery©2015 Cnes/Spot Image, DigitalGlobe, European Space Imaging, Landsat, Map data ©2015 Google) of the Bosco Fontana national park and the surroundings. The position of the flux tower is marked by a white cross and surrounded by the mean 80% of the flux footprint, which is represented by the white line (Acton et al., 2015) The dark green surrounding is the forest area of the national park.

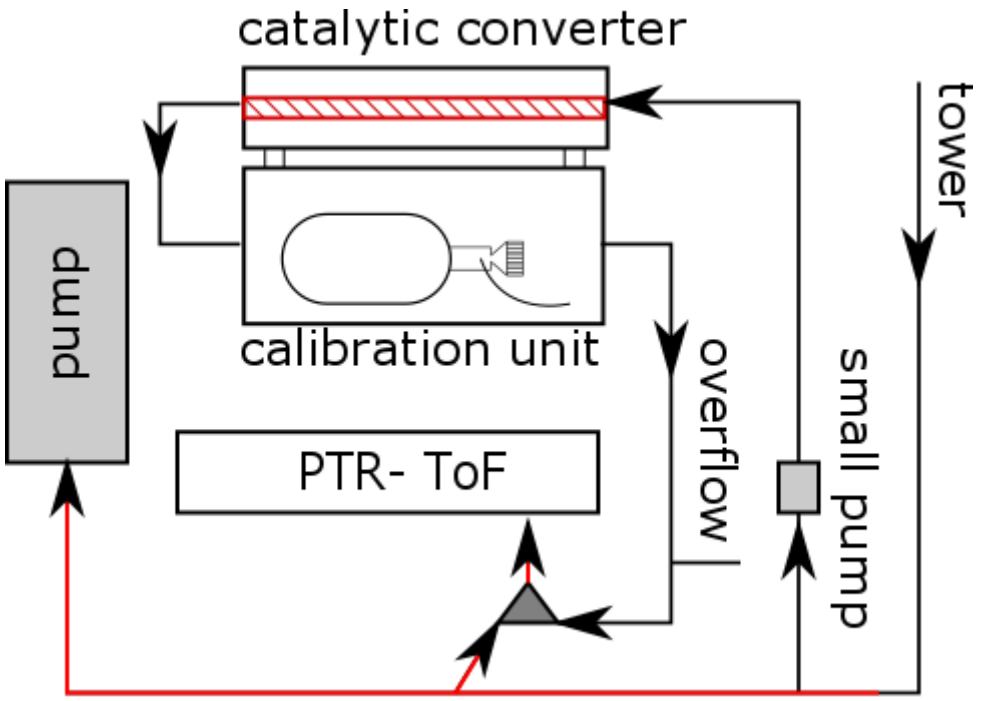

Figure 2: Schematic sketch of the inlet of the PTR-TOF used for the VOC measurements. Red lines indicade heated tubing.

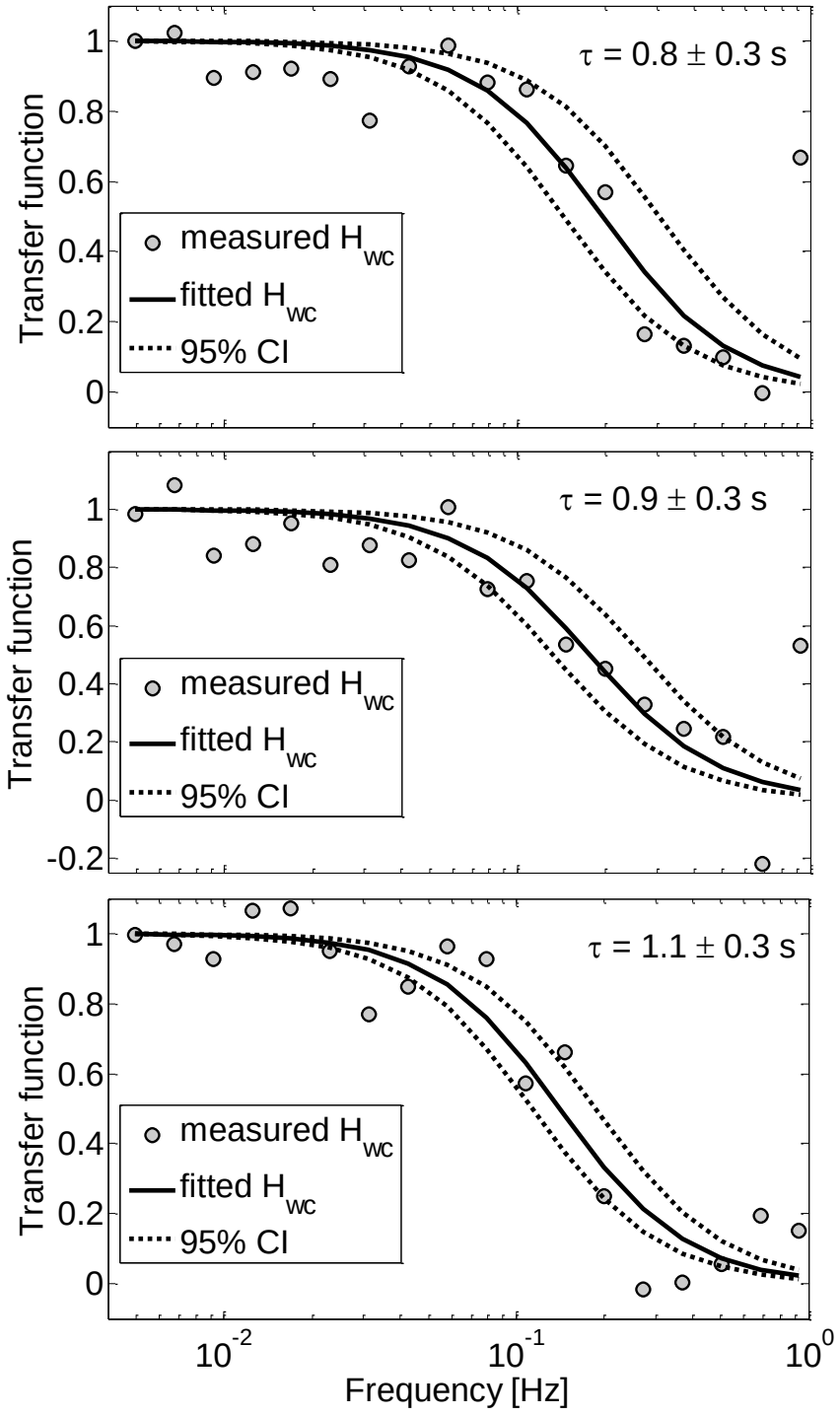

Figure 3: Transfer functions of $H_3O^+H_2O$ (37.0284 amu; top), $H_3O^+(H_2O)_2$ (55.039 amu; middle) and $C_5H_8H^+$ (69.0699 amu; bottom). The circles are the measurements, the solid black line the fitted transfer function and the dashed lines are the 95% confidence intervals. The response time of the measurement system, τ, was calculated by fitting Eq. 10 to the data.

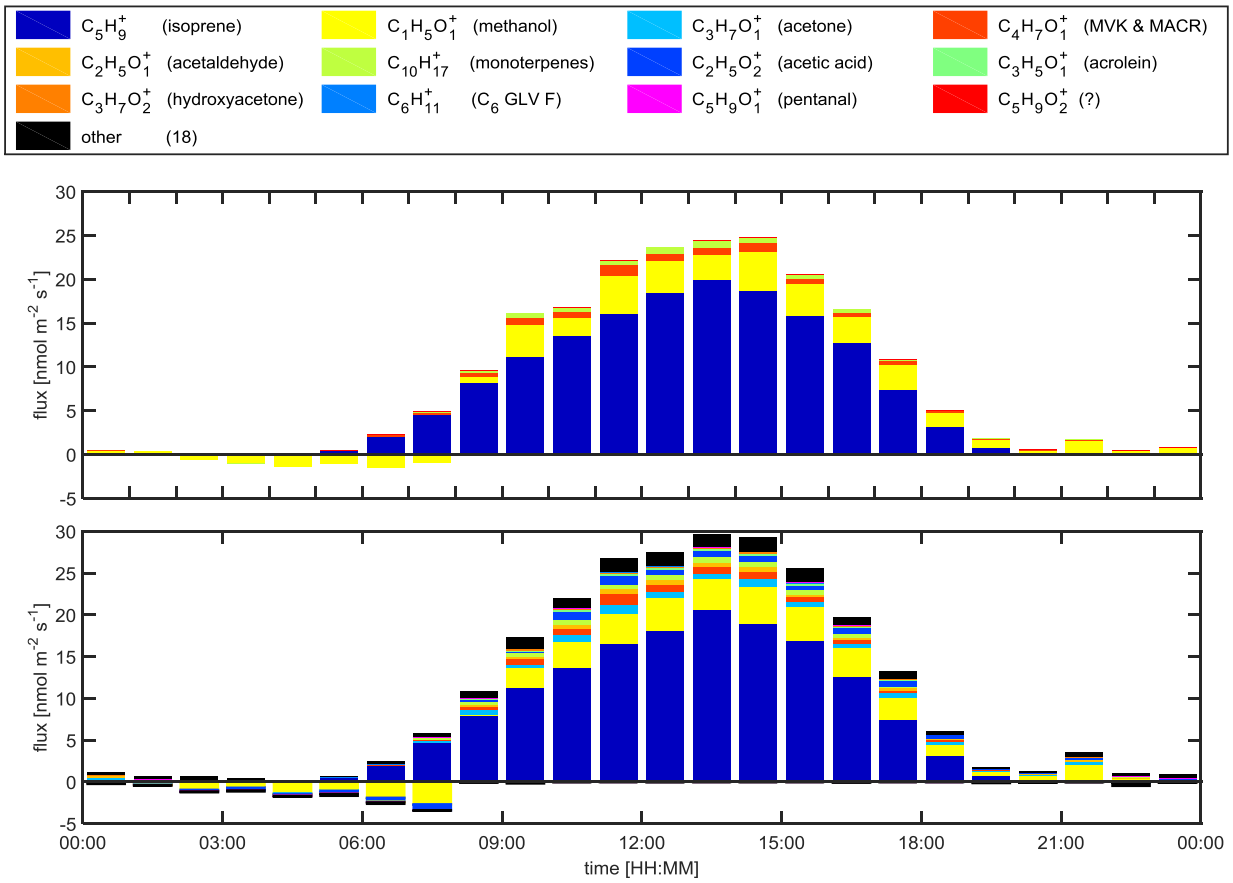

Figure 4: Diurnal flux plot of the classical method (top panel) and the automated method (bottom panel). For the automated method, the 10 $\boldsymbol{\sigma_{noise}}$ compounds are plotted individually, while the remaining 18 compounds, which passed the 3 $\boldsymbol{\sigma_{noise}}$ threshold (see Table A1), are summed up and plotted as 'other'. All individual flux compounds are listed in Table 2.

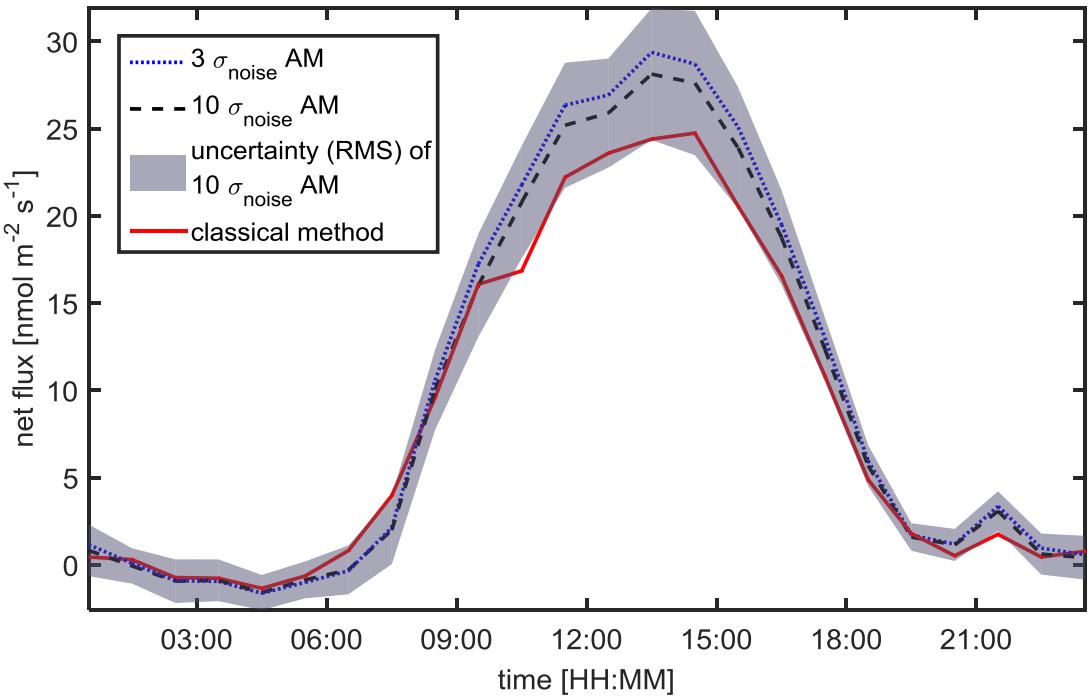

Figure 5: Diurnal net flux of the automated method (AM) with 3 and 10 σ_{noise} threshold for the flux calculation and the classical method. The uncertainty (root mean square) was calculated for the automated method with 10 σ_{noise}. The time is in CET wintertime.

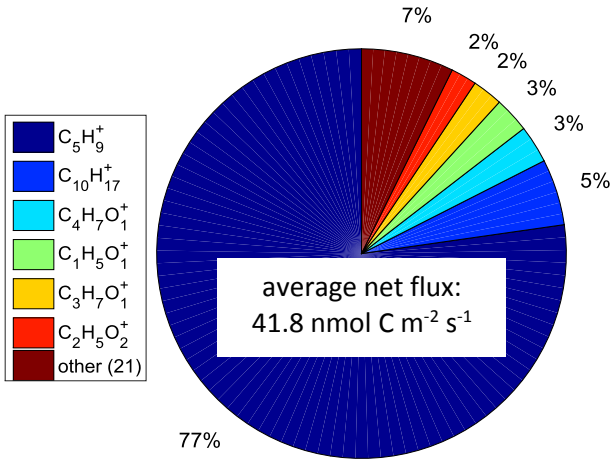

1 Figure 6: Average net flux of the major carbon emitters. Two masses were disregarded, as no matching
2 elemental composition was found.

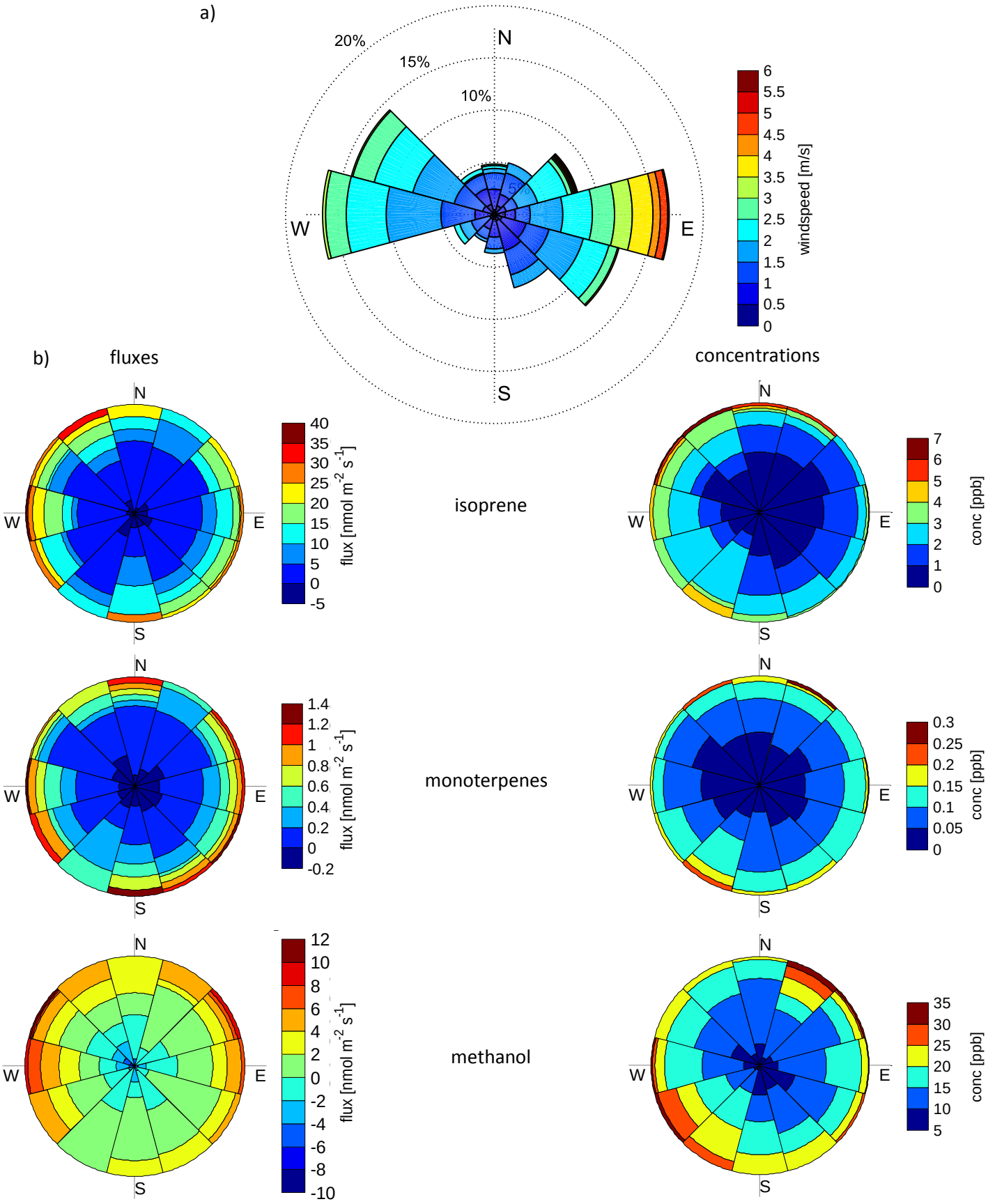

Figure 7: a) wind rose of the wind speed. The percentages describe the how often the wind came from the selected wind direction. b) Unscaled wind roses for fluxes (left) and concentrations (right) of isoprene (top), monoterpenes (mid), methanol (bottom).

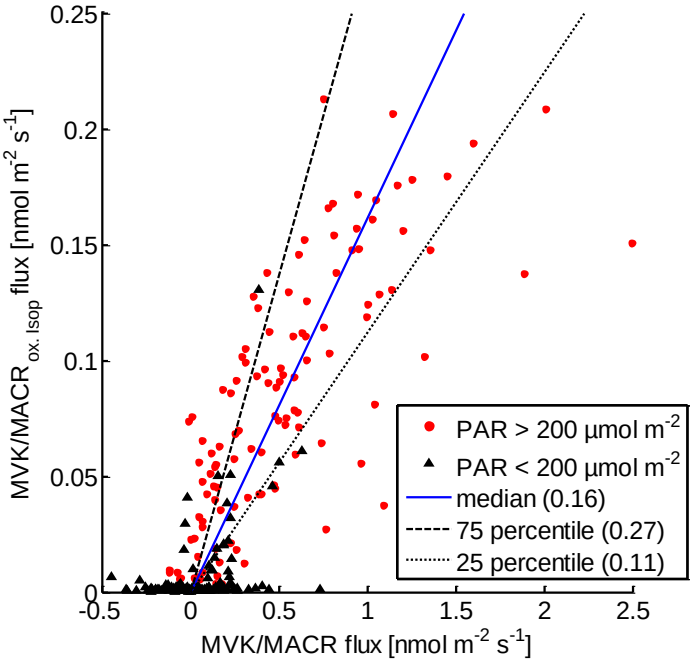

Figure 8: Scatter plot of the calculated MVK/MACR flux from oxidation of isoprene and the observed MVK/MACR flux. The correlation factor for the data is 0.81. The 1 h data are separated to day and night values by a 200 µmol m^{-2} photosynthetically active radiation (PAR) threshold. The $\frac{y}{x}$ ratios of the daytime data have been calculated to determine the median, 25th and 75th percentiles. The MVK/MACR flux from oxidation of isoprene was calculated using Eq. 14.

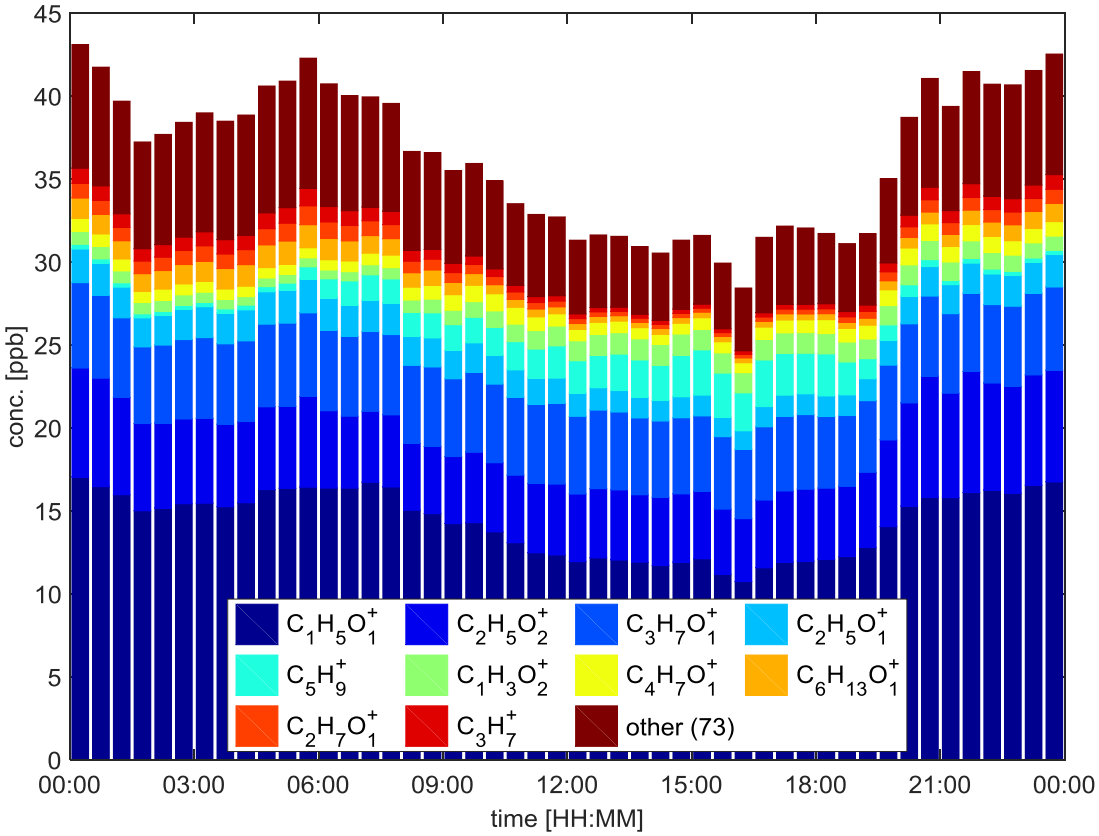

Figure 9: Diurnal average of the total VOC concentration resolved with the PTR-ToF (filtered for fragments). The 10 most abundend flux compounds are shown, the remaining compounds are summed up and plotted as 'other'.The time is in CET wintertime.

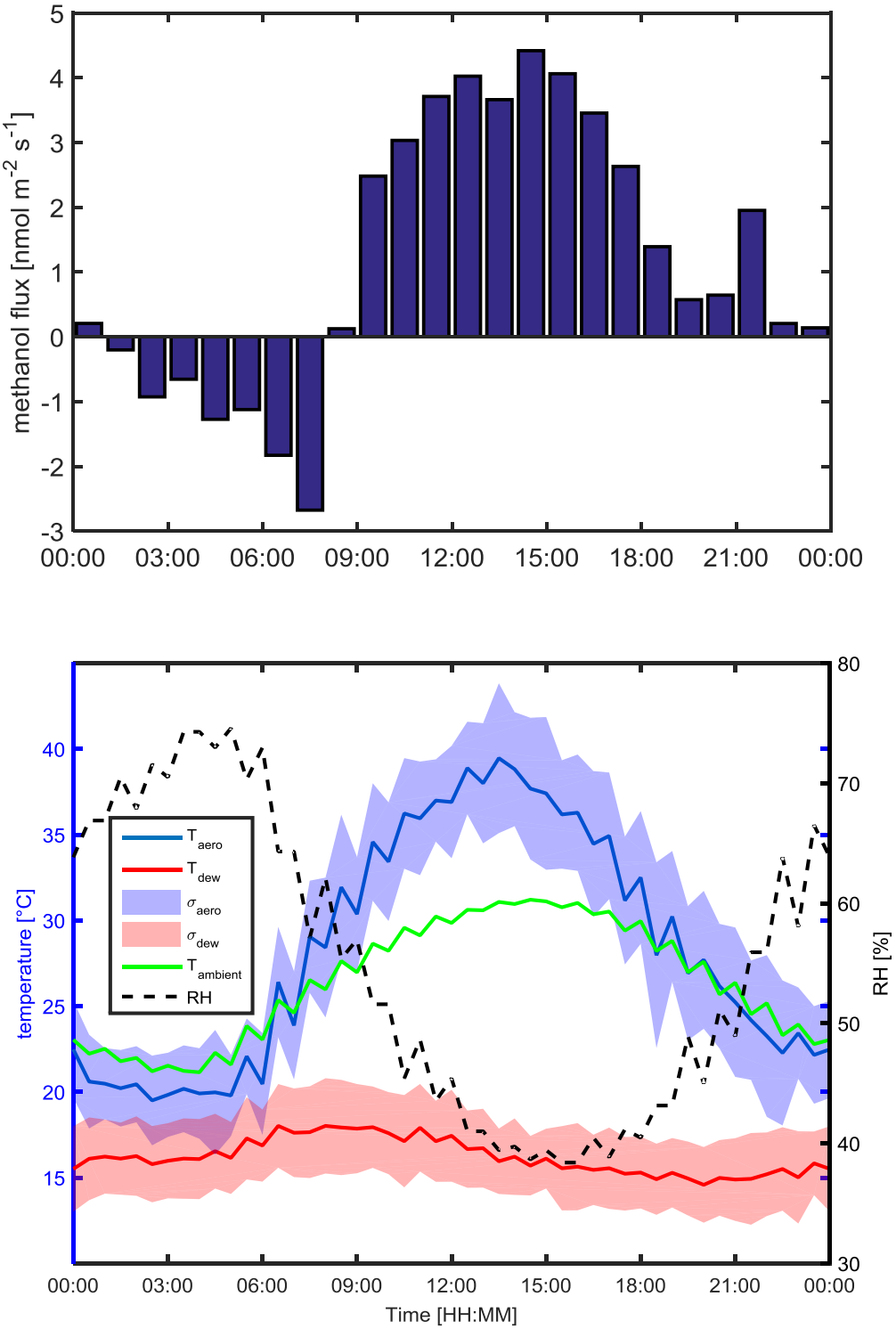

Figure 10: Diurnal exchange of the methanol (top panel) and the calculated aerodynamical (T_{aero}), dew point (T_{dew}) and ambient temperature ($T_{ambient}$; bottom panel).The shaded blue and red area indicades the standart deviation of the calculated temperatures and the dashed line is the relative humidity.

Appendix:

Table A1: Information about all measured 164 mass peaks in Bosco Fontana. The limit of detection is given for the calibrated masses. Masses with an F in the last column are filtered out as they were identified as fragments, clusters.

mass [amu]	elem. comp.	Background	sigma threshold	LOD (30min); Frag
21.0221		1	8.29	
27.0229	$C_2H_3^+$	1	-0.09	
28.0056	N_2^+	1	1.94	
29.0134	$H_1N_2^+$	1	35.03	
29.9974	$O_1N_1^+$	1	3.04	
31.0178	$C_1H_3O_1^+$	1	6.12	
31.9893	O_2^+	1	162.67	
32.9971	$H_1O_2^+$	1	3.42	
33.0335	$C_1H_5O_1^+$	0	45.69	38.5
35.0366	$H_5O_1N_1^+$	0	8.77	
36.0206	$H_4O_2^+$	1	1.98	
36.0444	$H_6O_1N_1^+$	1	19.26	
37.0284	$H_5O_2^+$	1	36.46	
38.0362	$H_6O_2^+$	1	159.67	
39.9629		1	1.42	
40.9710		1	1.74	
41.0386	$C_3H_5^+$	0	156.77	F
42.0100	$C_2H_2O_1^+$	0	-1.53	
42.0338	$C_2H_4N_1^+$	0	6.26	5.1
43.0178	$C_2H_3O_1^+$	0	10.57	F
43.0542	$C_3H_7^+$	0	5.13	
44.0138		0	1.74	
44.9971	$C_1H_1O_2^+$	1	2.63	
45.0335	$C_2H_5O_1^+$	0	15.53	13.2
45.9924	$O_2N_1^+$	1	3.27	
46.0287	$C_1H_4O_1N_1^+$	0	2.46	
47.0128	$C_1H_3O_2^+$	0	2.92	
47.0240	$H_3O_1N_2^+$	1	59.34	
47.0491	$C_2H_7O_1^+$	0	8.74	
48.0080	$H_2O_2N_1^+$	1	4.87	
49.0284	$C_1H_5O_2^+$	0	1.31	
49.9998	$H_2O_3^+$	1	-0.34	
51.0077	$H_3O_3^+$	1	5.73	
51.0441	$C_1H_7O_2^+$	0	26.53	F
51.9382		1	-1.63	
51.9944	$C_3O_1^+$	1	-0.68	
53.0022	$C_3H_1O_1^+$	1	-0.30	
53.0386	$C_4H_5^+$	0	3.59	
53.9394		1	-0.14	
55.0390	$H_7O_3^+$	1	167.77	
55.9377		1	2.88	
56.0468	$H_8O_3^+$	1	7.35	
57.0335	$C_3H_5O_1^+$	0	19.26	6.9

57.0699	$C_4H_9^+$	1	12.76	
57.9352		1	-0.86	
59.0491	$C_3H_7O_1^+$	0	15.82	6.1
60.0481		0	1.42	
61.0284	$C_2H_5O_2^+$	0	11.79	
62.0237	$C_1H_4O_2N_1^+$	0	0.84	
63.0263	$C_2H_7S_1^+$	0	1.60	
63.9852	$H_2O_1N_1S_1^+$	0	-1.30	
65.0233	$C_1H_5O_3^+$	0	5.84	
65.0584	$H_7O_1N_3^+$	0	1.59	
67.0542	$C_5H_7^+$	0	64.76	F
68.0621	$C_5H_8^+$	0	96.03	F
69.0699	$C_5H_9^+$	0	241.62	2.8
71.0491	$C_4H_7O_1^+$	0	39.95	4.7
71.0851	$C_5H_{11}^+$	0	7.47	
72.0875		0	6.68	
73.0255		0	3.63	
73.0473		0	0.73	
73.0648	$C_4H_9O_1^+$	0	9.64	2.1
74.0227		0	0.75	
75.0441	$C_3H_7O_2^+$	0	11.07	
75.9436	$C_1S_2^+$	1	0.51	
77.9424		1	-0.60	
79.0542	$C_6H_7^+$	0	3.44	2.5
80.9971	$C_4H_1O_2^+$	0	-0.80	
81.0335	$C_5H_5O_1^+$	1	10.76	
81.0699	$C_6H_9^+$	0	106.38	F
83.0523		0	1.47	
83.0855	$C_6H_{11}^+$	0	15.80	
85.0284	$C_4H_5O_2^+$	0	1.50	
85.0648	$C_5H_9O_1^+$	0	12.14	
85.1012	$C_6H_{13}^+$	0	1.30	
85.9471		1	1.27	
87.0441	$C_4H_7O_2^+$	0	1.58	
87.0804	$C_5H_{11}O_1^+$	0	1.61	
88.0763		0	1.14	
88.9555	$H_3O_1Cl_2^+$	1	0.42	
89.0233	$C_3H_5O_3^+$	0	3.58	
89.0597	$C_4H_9O_2^+$	0	0.99	
90.9487		1	7.58	
91.0567		0	1.16	
91.9457		1	1.79	
92.9480		1	2.59	
93.0369	$C_3H_9O_1S_1^+$	1	6.19	
93.0699	$C_7H_9^+$	0	1.79	0.7
93.9542	$C_1H_2O_1S_2^+$	1	-2.91	
95.0161	$C_2H_7O_2S_1^+$	0	-0.06	
95.0478	$C_4H_5N_3^+$	0	1.20	
95.0855	$C_7H_{11}^+$	0	8.87	F
95.9512	$O_4S_1^+$	1	1.38	

96.9961		0	1.10	
97.0284	$C_5H_5O_2^+$	0	3.04	
97.0634	$C_4H_7N_3^+$	0	2.96	
97.1012	$C_7H_{13}^+$	0	1.00	
98.0237	$C_4H_4O_2N_1^+$	1	-1.51	
98.0600	$C_5H_8O_1N_1^+$	0	1.43	
99.0077	$C_4H_3O_3^+$	0	0.34	
99.0441	$C_5H_7O_2^+$	0	6.23	
99.0804	$C_6H_{11}O_1^+$	0	6.69	
100.0393	$C_4H_6O_2N_1^+$	1	0.08	
100.0757	$C_5H_{10}O_1N_1^+$	1	-0.90	
101.0233	$C_4H_5O_3^+$	0	-1.69	
101.0597	$C_5H_9O_2^+$	0	5.07	
101.0961	$C_6H_{13}O_1^+$	0	3.11	18.7
101.9428		0	0.35	
102.0913	$C_5H_{12}O_1N_1^+$	0	0.57	
102.9468		0	-0.23	
103.0390	$C_4H_7O_3^+$	0	1.35	
103.0754	$C_5H_{11}O_2^+$	0	2.90	
103.9516	$H_5S_2Cl_1^+$	1	0.17	
105.9359		1	1.19	
106.9418		1	0.07	
106.9617		0	0.61	
107.0491	$C_7H_7O_1^+$	0	1.47	
107.0855	$C_8H_{11}^+$	0	0.58	0.4
107.9512	$C_1O_4S_1^+$	1	2.75	
108.9590	$C_1H_1O_4S_1^+$	1	2.88	
108.9920	$C_5H_1O_3^+$	1	-0.03	
109.0284	$C_6H_5O_2^+$	0	-3.77	
109.0648	$C_7H_9O_1^+$	0	2.71	
109.1012	$C_8H_{13}^+$	0	1.06	
111.0441	$C_6H_7O_2^+$	1	1.08	
111.0804	$C_7H_{11}O_1^+$	1	1.28	
111.1168	$C_8H_{15}^+$	0	-0.31	
111.9461	$O_5S_1^+$	1	-0.89	
113.0597	$C_6H_9O_2^+$	0	-0.83	
113.0947	$C_5H_{11}N_3^+$	0	2.37	
115.0096		1	1.31	
115.0363	$C_1H_3O_1N_6^+$	0	-1.02	
115.0754	$C_6H_{11}O_2^+$	0	2.18	
115.1117	$C_7H_{15}O_1^+$	0	-0.24	
116.9060	$C_1Cl_3^+$	0	-0.28	
117.9542	$C_3H_2O_1S_2^+$	1	-2.30	
118.9451		0	-3.19	
119.9512	$C_2O_4S_1^+$	1	-0.03	
120.9534		0	-1.06	
121.0648	$C_8H_9O_1^+$	0	0.10	
121.1012	$C_9H_{13}^+$	0	0.78	0.4
123.0441	$C_7H_7O_2^+$	1	0.20	
123.1168	$C_9H_{15}^+$	0	1.78	

123.9440		1	10.14	
124.9510	$C_1O_4N_1Cl_1^+$	1	-1.66	
125.9572		1	-0.85	
126.0159	$C_2H_6O_6^+$	1	1.45	
126.0557		1	1.71	
126.0957		1	0.30	
127.0390	$C_6H_7O_3^+$	0	1.84	
127.0754	$C_7H_{11}O_2^+$	1	-1.93	
127.1117	$C_8H_{15}O_1^+$	0	-0.12	
128.1107		1	-0.39	
130.9920		1	1.39	
135.0406		0	4.35	
137.0557		0	2.16	
137.1325	$C_{10}H_{17}^+$	0	115.45	0.5
138.0590		1	30.15	
140.0304		1	1.14	
140.0751		1	-1.76	
144.9606	$C_6H_3Cl_2^+$	1	0.69	
145.9685	$C_6H_4Cl_2^+$	1	-0.02	
180.9373	$Cl_3C_6H_4^+$	1	2.40	

1

Table A2: comparison of the detected compounds with flux in Bosco Bontana and their values at the orange grove (Park et al., 2013).

Elemental composition	mass [amu]	net (downward/ upward) flux (24h average) [nmol m-2 s-1] this study	Park et al., (2013)[1]
$C_1H_5O_1^+$	33.0335	1.168 (-0.365/1.533)	1.655 (-0.102/1.757)
$H_5O_1N_1^+$	35.0366	0.061 (-0.002/0.064)	
$C_2H_4N_1^+$	42.0338	0.046 (-0.005/0.051)	
$C_3H_7^+$	43.0542	0.079 (-0.005/0.084)	0.075 (-0.001/0.076)
$C_2H_5O_1^+$	45.0335	0.228 (-0.001/0.229)	0.133 (-0.016/0.148)
$C_2H_7O_1^+$	47.0491	0.105 (-0.02/0.125)	-0.013 (-0.017/0.004)
$C_4H_5^+$	53.0386	0.008 (-0.001/0.009)	0.012 (-0.009/0.021)
$C_3H_5O_1^+$	57.0335	0.085 (-0.002/0.086)	0.033 (-0.016/0.049)
$C_3H_7O_1^+$	59.0491	0.335 (-0.01/0.345)	0.281 (-0.004/0.286)
$C_2H_5O_2^+$	61.0284	0.214 (-0.096/0.311)	0.413 (-0.005/0.418)
$C_1H_5O_3^+$	65.0233	0.03 (-0.001/0.031)	
$C_5H_9^+$	69.0699	6.466 (0/6.466)	0.025 (-0.001/0.025)
$C_4H_7O_1^+$	71.0491	0.311 (-0.004/0.315)	0.041 (-0.004/0.044)
C_5H_{11}+	71.0851	0.02 (-0.001/0.021)	0.006 (-0.005/0.011)
unknown	72.0875	0.015 (-0.002/0.016)	
unknown	73.0255	0.026 (-0.009/0.035)	
$C_4H_9O_1^+$	73.0648	0.075 (-0.002/0.077)	0.029 (-0.007/0.036)
$C_3H_7O_2^+$	75.0441	0.068 (-0.005/0.073)	
$C_6H_7^+$	79.0542	0.021 (-0.002/0.023)	0.016 (-0.002/0.018)
$C_6H_{11}^+$	83.0855	0.034 (0/0.035)	0.007 (-0.004/0.011)
$C_5H_9O_1^+$	85.0648	0.017 (-0.001/0.018)	0.008 (-0.005/0.013)
$C_3H_5O_3^+$	89.0233	0.011 (-0.001/0.012)	0.007 (-0.004/0.011)
$C_5H_5O_2^+$	97.0284	0 (-0.002/0.002)	0.007 (-0.005/0.012)
$C_4H_7N_3^+$	97.0634	0.003 (-0.001/0.004)	0.007 (-0.007/0.015)
$C_5H_7O_2^+$	99.0441	0.017 (-0.001/0.018)	0.008 (-0.004/0.012)
$C_6H_{11}O_1^+$	99.0804	0.014 (-0.001/0.014)	
$C_5H_9O_2^+$	101.0597	0.014 (-0.001/0.014)	0.004 (-0.003/0.008)
$C_6H_{13}O_1^+$	101.0961	0.091 (-0.037/0.128)	
$C_{10}H_{17}^+$	137.1325	0.219 (-0.001/0.219)	0.235 (0/0.236)[2]

[1] the presented data was calculated from Table S2 in the supplement.

[2] the fragments of monoterpenes were summed up to compare it with upscaled monoterpene signal from B.F.

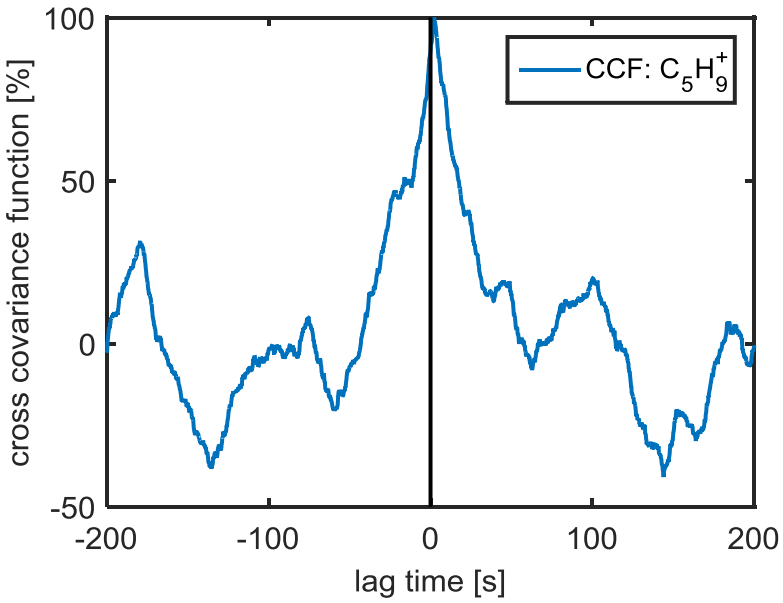

Fig A1: 30 min cross covariance function of $C_5H_9^+$ from the 15.06.2012 14:15. The function was normalized to the maximum. A clear maximum can be seen, slightly shifted to the right by the lag time.

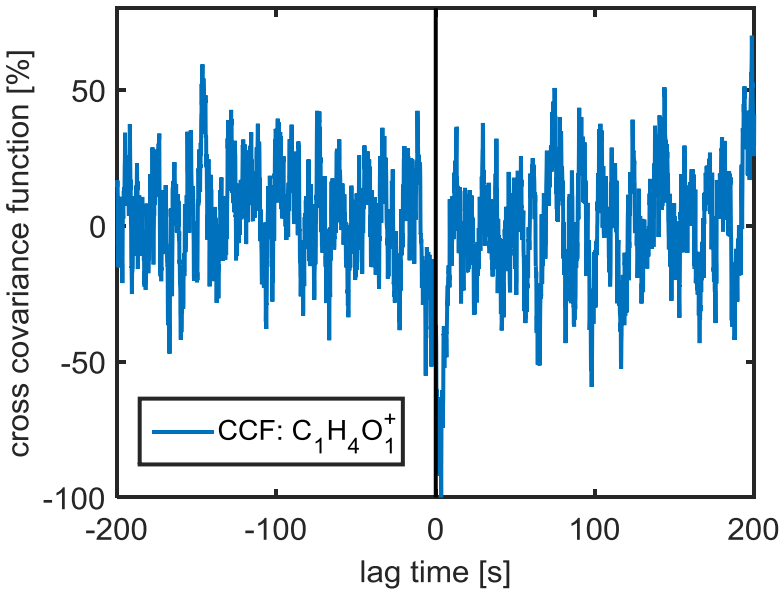

Fig A2: 30 min normalized cross covariance function of $C_1H_4O_1^+$ from the 22.06.2012 04:45. A clear minima can be seen, which defines downward fluxes.

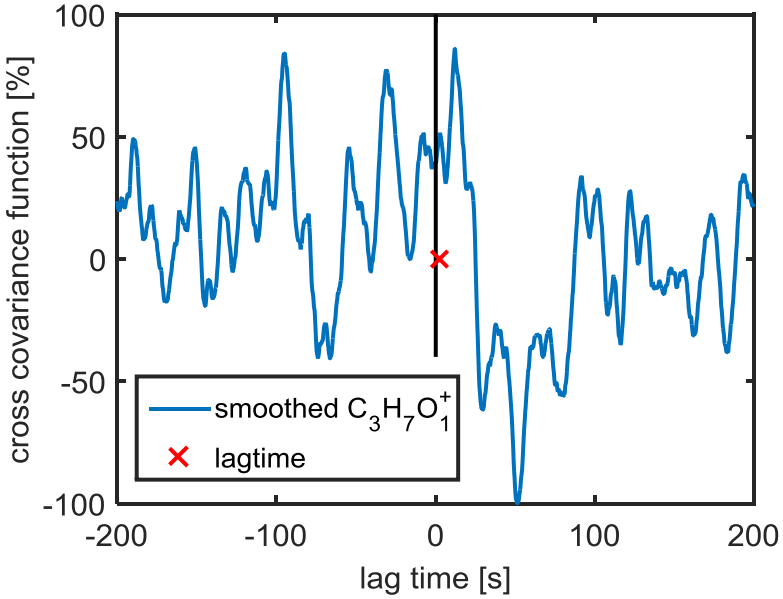

Fig S A3: Smoothed normalized CCF of $C_3H_7O_1^+$. The red cross marks the lagtime used in the original CCF (Fig A4) to find the flux value the allowed lagtime window is from 0 s to 5 s. In this specific CCF only a local maximum was found, as there is no clear maximum.

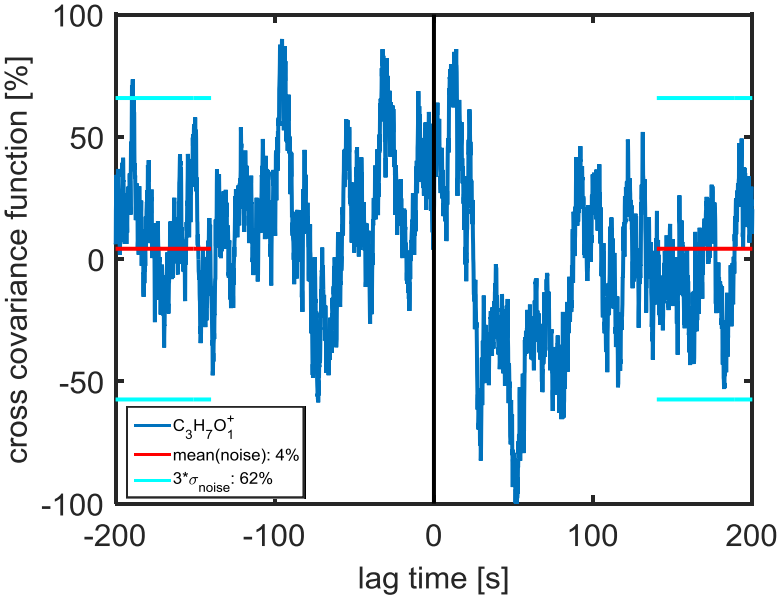

Fig A4: 30 min normalized cross covariance function of $C_3H_7O_1^+$ from the 15.06.2012 14:15. No clear maximum or minimum can be seen around 0 s lag time. The red lines at the corners of the plot indicate the average noise, while the cyan lines are the 3 σ_{noise} threshold (in the legend the 62% represents just the 3 σ_{noise}, while in the plot it is added to the mean noise).

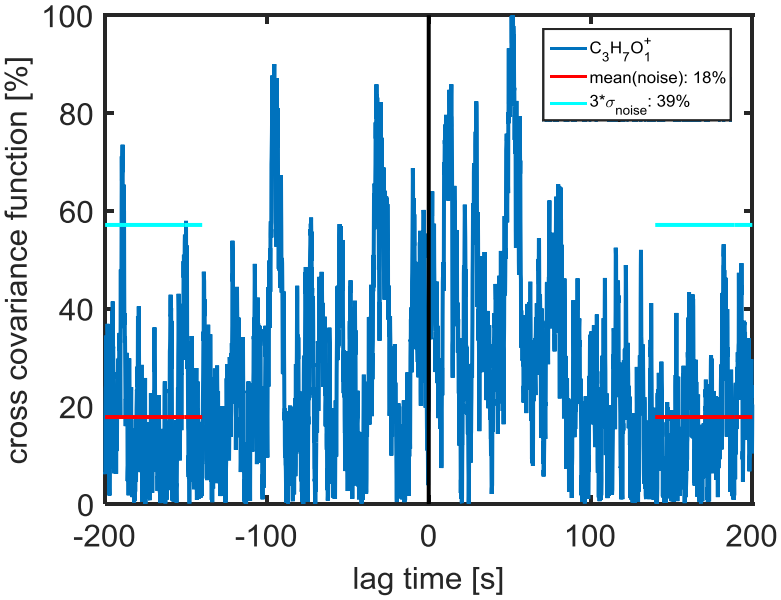

Fig A5: 30 min absolute normalized cross covariance function of $C_3H_7O_1^+$ from the 15.06.2012 14:15. The red lines at the corners of the plot indicate the average noise, while the cyan lines are the 3 σ_{noise} threshold (in the legend the 39% represents just the 3 σ_{noise}, while in the plot it is added to the mean noise). Taking the absolute of a CCF increases the mean value and thereby reduces the standard deviation of the noise (compare with Fig. A4)

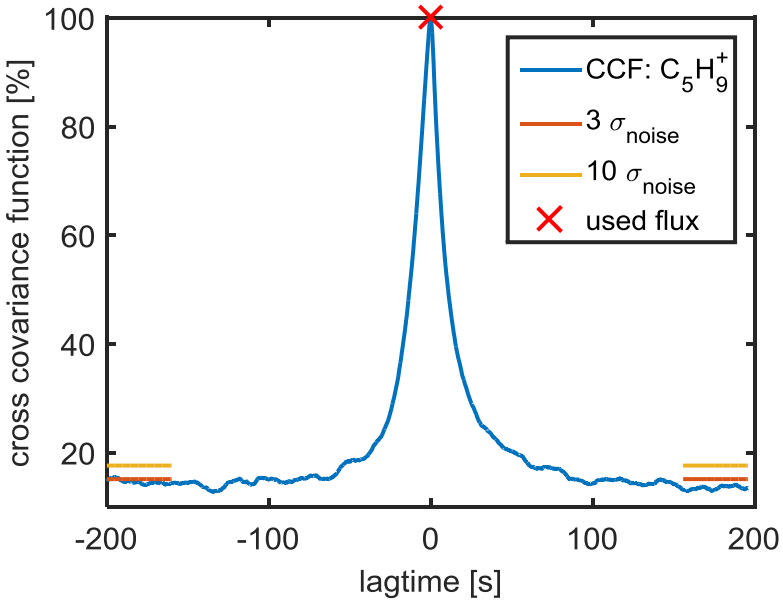

Figure A6: Averaged absolute CCF for $C_5H_9^+$. The used flux is well over the 10 σ_{noise} criteria.

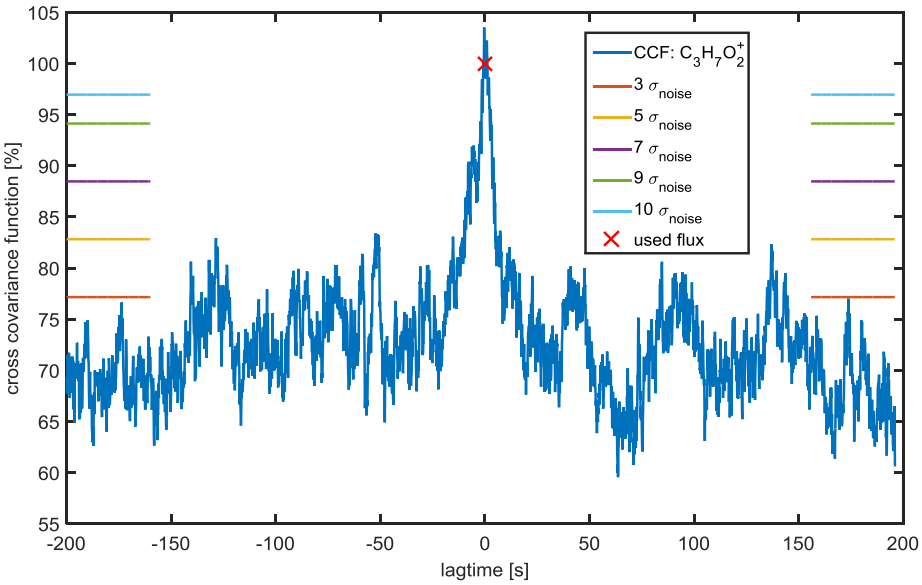

Figure A7: Averaged absolute CCF for $C_3H_7O_2^+$. Due to the constant lag time, not always the maximum of the CCF is used, as this would overestimate the flux. In this case the used value is actually a local minimum between two maxima.

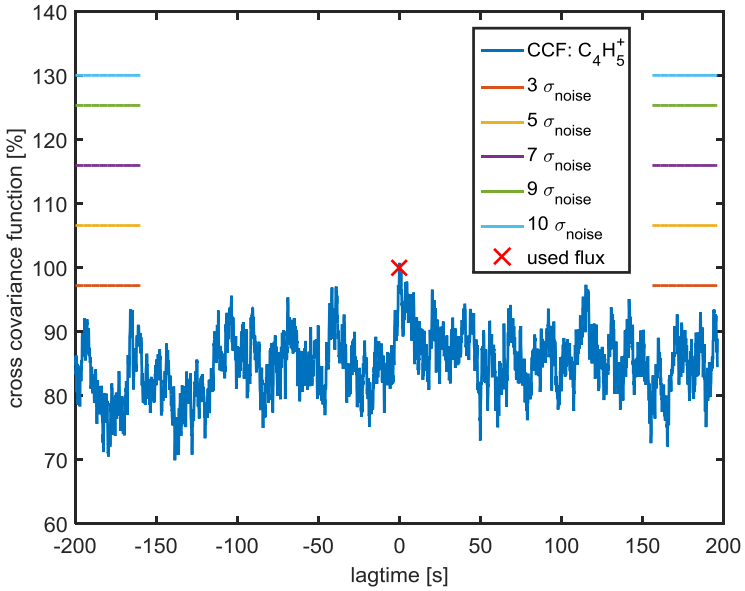

Figure A8: Averaged absolute CCF of $C_4H_5^+$, which fulfilled the 3 σ_{noise} criteria.

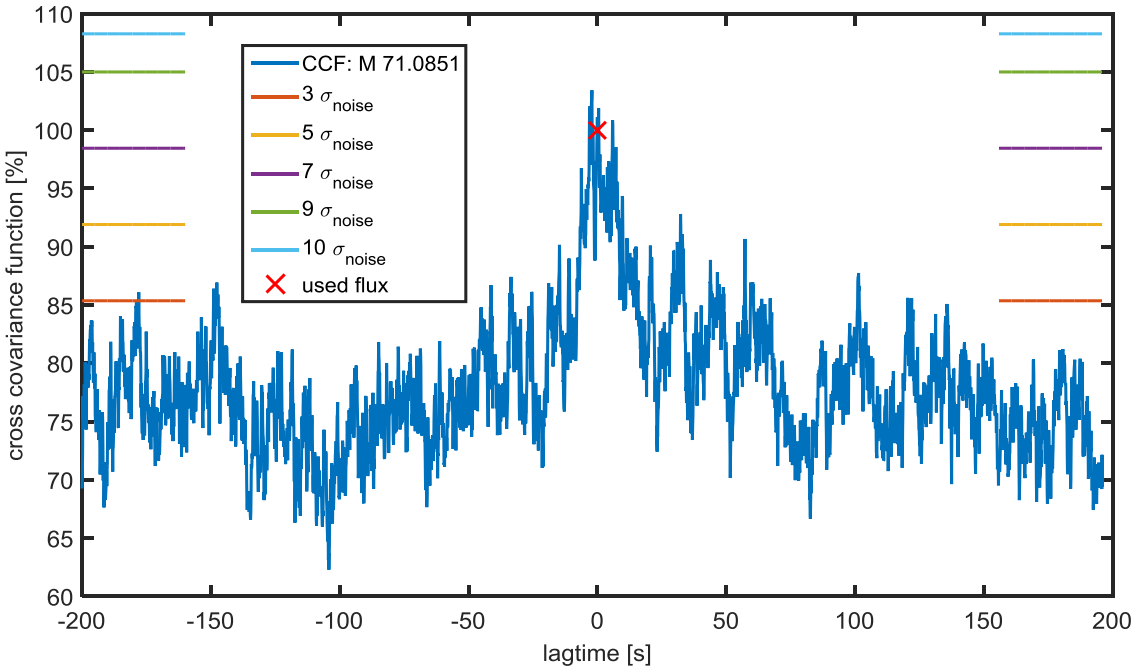

Figure A9: Averaged absolute CCF of mass 71.0851 (could not be identified), which fulfilled the 7 σ_{noise} criteria.